UNDER-LIQUID WETTING DYNAMICS

SURJYASISH MITRA

A THESIS SUBMITTED TO THE FACULTY OF
GRADUATE STUDIES IN PARTIAL FULFILLMENT OF
THE REQUIREMENTS FOR THE DEGREE OF MASTER
OF APPLIED SCIENCE

GRADUATE PROGRAM IN MECHANICAL ENGINEERING
YORK UNIVERSITY
TORONTO, ONTARIO

August 2016

Abstract

Liquid drops wetting a surface kept in ambient air has been widely studied over the last few decades due to its manifold applications in technology and industry. However, for a surface kept submerged under-liquid, such wetting processes have been studied to a lesser extent. Understanding how a liquid drop interacts with a surface in the presence of another liquid medium is pivotal towards growing applications in marine ecosystem, environmental effects of oil-spills, advanced manufacturing techniques like immersion lithography, etc. It also poses the challenging issues of liquid-liquid displacement and contact line dynamics. The present study delineated some fundamentals of under-liquid wettability like coalescence of two sessile drops on an under-liquid substrate, spreading of liquid drops on an under-liquid substrate and drop interaction with submerged micro-patterned substrates. Through relevant theoretical analysis as well as experimentation, it was found that the existing theories of drop interaction with a surface in air are inadequate when a surrounding liquid medium is considered, and needs to be modified bringing into effect key parameters of the surrounding medium, such as its density and viscosity. Consideration of a surrounding liquid medium also allows to provide a unifying framework to study such wetting processes. For coalescence and spreading, a universal behavior was observed in terms of the initial fast wetting regime inherent to such processes, and the notion of coalescence-spreading analogy was found acceptable to describe such phenomenon. However, for under-liquid wetting signature of micro-patterned substrates, a non-universal behavior was observed which indicates the need of newer theoretical approach to better understand wetting phenomenon on such under-liquid surfaces.

Acknowledgments

I would like to take this opportunity to thank everyone who has helped me throughout my graduate studies. First and foremost, I would like to express my deepest gratitude to my thesis supervisor, Dr. Sushanta Mitra, for his continuous guidance, enthusiasm, support, and timely encouragement throughout my graduate studies.

I would like to thank my supervisory committee member, Dr. George Zhu for his valuable suggestions.

I am grateful to the Natural Sciences and Engineering Research Council (NSERC) of Canada for the financial support through research grants.

I am thankful to all past and present members of Micro Nano Transport Laboratory (MNTL), Saumyadeb Dasgupta, Dr. Naga Siva Kumar Gunda, Ravi Chavali and Dr. Bichitra Nanda Sahoo for their co-operation and useful discussions. I would like to specially thank Dr. Naga Siva Kumar Gunda, post doctoral fellow at MNT Lab, for fabricating the micro-patterned substrates for the 'under-liquid wetting on micro-patterned substrates' study.

Finally, I would like to express my sincere thanks to my parents, Mr. Sasanka Mitra and Mrs. Mita Mitra, my brother, Debasish Mitra and my friends Sudhira, Sabyasachi, Apratim, Siddhartha, Deeptarka, Arunima, Arita, Aniket and Souravik for their patience, encouragement, understanding and continuous support.

Contents

List of Tables

List of Figures

Nomenclature and Abbreviations

Greek Letters

ρ_D	Density of the liquid drop
ρ_L	Density of the surrounding liquid
μ_D	Dynamic viscosity of liquid drop
μ_L, μ_S	Dynamic viscosity of surrounding liquid
γ_{DA}, γ_{LA}	Surface tension of liquid/liquid drop in air
γ_{DW}	Interfacial tension of liquid drop with water
θ_0, θ_E, θ_{eq}	Equilibrium contact angle (Young's)
θ_{Wenzel}	Wenzel contact angle
θ_{CB}	Cassie-Baxter contact angle
θ_A	Advancing contact angle
θ_R	Receding contact angle
ϕ	Cassie fraction
α	Scaling exponent

Latin letters

h_0	liquid bridge height
R, R_0	radius of liquid drop
l_v	viscous length scale
p_D	pressure of liquid drop
p_L	pressure in the surrounding liquid
p_A	ambient air pressure

Abbreviations

TPCL	Three phase contact line
DBP	Dibutyl Pthalate

Chapter 1

Introduction

1.1 Motivation

Wetting phenomenon is a fundamental multi-disciplinary research area having a delicate mix of physics, chemistry, mathematics, material science and engineering. Wetting refers to the interaction of two fluids (liquid-gas or liquid-liquid) with a surface due to the intermolecular forces between them [1, 2]. Wetting can occur across different length scales: on large scales we can relate to the drainage of water from flood-hit streets or giant waves crashing on the beach where as on small scales, we encounter familiar events like how raindrops falling on leaves or our car windshields settle down forming a typical spherical cap shape or how a coffee stain is left behind upon evaporation of coffee drops from our clothes[3, 4]. Nature offers many more such fascinating examples of wetting phenomenon (see Fig. 1.1). Water flowing down our kitchen faucet breaks up into a train of drops by the virtue of surface tension driven instability [5]. A lotus leaf (or a taro leaf) due to its micro-nano hierarchical structures can repel water drops and contaminants easily from its surface, the so called Lotus effect[6]. Water strider (Gerris remigis) shows remarkable behavior of walking and gliding on water surface which can be attributed to

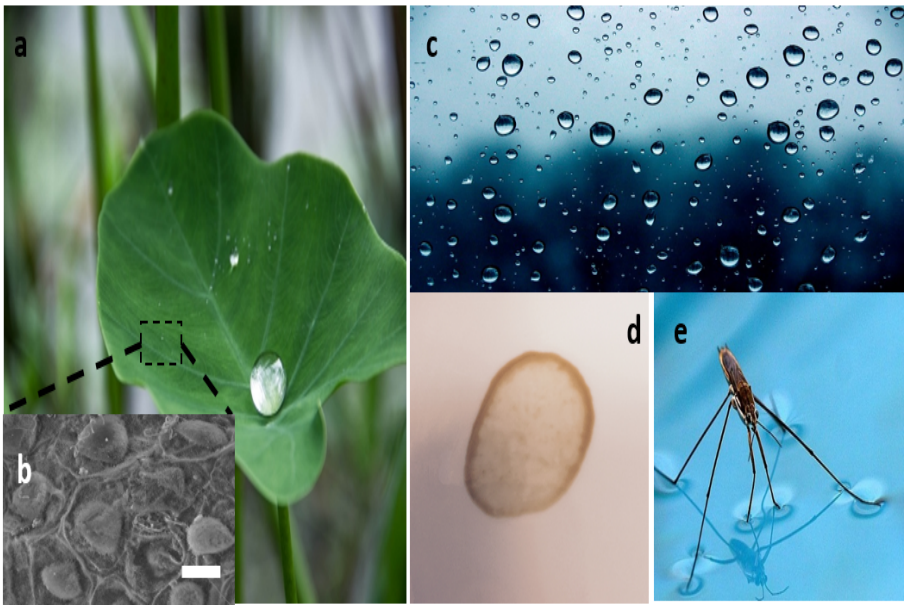

Figure 1.1: (Color online) Wetting phenomena in nature. (a) Water drop sitting on a *taro* leaf. (b) A typical SEM micrograph of a cross-section of a *taro* leaf showing the textured nature of the surface. The scale bar represents 20μm. (c) Rain drops on a window pane representing the spherical cap geometry. (d) A coffee stain formed upon evaporation of a coffee drop. (e) A water strider standing on water.

the role of surface tension generated force around the curved water-air interface coupled with its hydrophobic legs that supports its weight [7, 8, 9]. Not only does wetting offers such fascinating physics in our day to day lives, but it is also relevant to many technological applications. Studies involving wetting dynamics on small scales, i.e., spreading[1, 10, 11], coalescence[12], impact of small drops [13, 14] or manipulation of small drops in a variety of settings[15] have direct consequences in numerous applications: from inkjet printing, powder metallurgy [16], droplet microfluidics (lab on chip devices) [15, 17, 18] to applications in oil recovery [19, 20, 21, 22, 23]. For example, Drop on Demand (DOD) inkjet printing is based on the formation and manipulation of a single ink drop upon actuation of a print head [24, 25]. The drainage of oil residue from porous rocks depends on the wetting properties of oil in presence of surrounding gas phase, water phase and the porous media [23]. With the recent advent

of microfluidics, there has been a surge in the study of discrete liquid drops or bubbles in micro-scale environment applicable for advanced drug delivery[26], bio-medical devices for diagnostic testing [27, 28], etc. However, till date, most studies involving wetting processes have been performed for surfaces kept in ambient air, i.e., phenomenon such as spreading, impact of liquid drops on surfaces kept in ambient air or coalescence of two drops kept on a surface in air. Growing applications pertaining to underwater environment like understanding effects of oil-spills and prevention of its adverse effects, appropriate design of marine pipelines, low drag surfaces like submerged ship parts, etc, have made it indispensable to perform a more generalized study of this phenomenon taking into consideration a dynamically active environment (i.e., a surrounding viscous liquid for this case). The present research aims to address some of the fundamental aspects related to under-liquid wetting dynamics.

1.2 Main Topics

1.2.1 Coalescence of liquid drops

From raindrop formation in clouds to advanced manufacturing techniques like lithography, coalescence of two liquid drops is a fundamental process where two liquid drops on being brought together merge and form a composite drop. The underlying physics of such merging process comes from the fact that the two drops effectively minimizes its surface area by forming a composite drop when brought in contact. Frenkel(1945) was the first to study the phenomenon of drop coalescence (pendant drops in this case) - in air and concluded that such coalescence is dictated by viscous forces within the drop, which can be described by the Stokes equations [29]. Since then, physics of drop coalescence has been investigated experimentally and theoretically much extensively for sus-

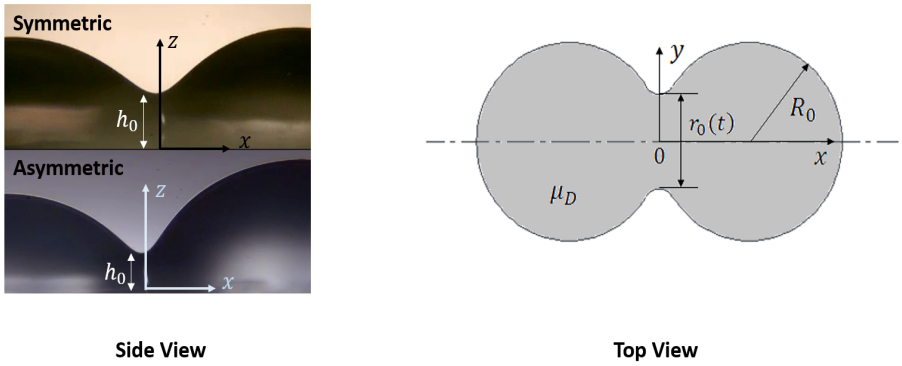

Figure 1.2: (Color online) Coalescence of sessile drops. Schematic showing the coalescence process from side view and top view. $h_0(t)$ represents the liquid bridge height formed upon the merging of the two drop. $r_0(t)$ represents the liquid bridge width.

pended (pendant) drops [12, 30, 31, 32, 33, 34, 35, 36, 37, 38, 39, 40, 41] and and to a lesser extent for drops in contact with a substrate (sessile drops) [42, 43, 44, 45, 46]. When two spherical drops are deposited on a substrate and are allowed to merge, a small liquid bridge forms connecting the two drops, which rapidly grows due to liquid flux from the drops towards the bridge region [47, 48, 12]. This initial rapid motion is followed by a slow merging of the two drops [42]. The shape evolution and flows within the drops during the merging process are dictated by a balance between surface tension, viscosity and inertial forces. Irrespective of the liquid properties, the coalescence process always begins in a regime dominated by drop viscosity while at later times of coalescence inertial effect takes over [41, 12, 40]. In that regard, the characteristic flow Reynolds No. and the characteristic viscous length scale play an important role in dictating the nature and extent of the initial regime. Some of the earlier works on sessile drop coalescence focused on the growth of the liquid bridge connecting the two drops in the horizontal plane. It was found that for high viscosity drops, the bridge neck radius r(t) grows with time following a scaling, $r \sim t^{1/2}$. Even though from a top view perspective, the coalescence of two sessile drops is similar to that of pendant drop coalescence [12, 49],

however, the coalescence process when viewed from side shows an entirely different picture due to the additional presence of the substrate [42, 43, 44, 45]. It was recently shown by Hernández-Sánchez et al. [43] that when two sessile drops (of high viscosity liquids) merge on a glass substrate (completely wetting condition), an infinitesimally small liquid bridge forms, which develops a self-similar profile and the bridge height grows linearly as $h_0 \sim t$. They also showed that even though the process is three-dimensional, it can be effectively modeled using the one-dimensional lubrication theory for viscous flows [50, 12]. However, it should be noted that, till date, all studies on sessile drop coalescence has been performed in an ambient air medium. In many real life applications, drops merge on a substrate in the presence of a surrounding viscous medium [51]. Often, pollutants like oil spills from tankers and off-shore drilling facilities interact with under-water marine and freshwater ecosystems. To analyze such interactions and accordingly design appropriate under-water substrates to mitigate environmental pollution [52], a fundamental understanding of drop coalescence on an under-liquid substrate is required.

1.2.2 Spreading of liquid drops

A liquid drop on contact with a given surface spreads due to unbalanced interfacial tension till equilibrium is reached. The final shape of the drop is characterized by a spherical cap geometry (see Fig. 1.4c) with equilibrium contact angle θ_{eq}, given by the Young's equation [1],

$$cos\theta_{eq} = \frac{\gamma_{SV} - \gamma_{SL}}{\gamma_{LV}} \tag{1.1}$$

Over the last few decades, the spreading process in ambient air has been widely studied due to its relevance in technological processes such as coating and painting [53], surface characterization [54, 55], biomimmetics[56, 57], inkjet print-

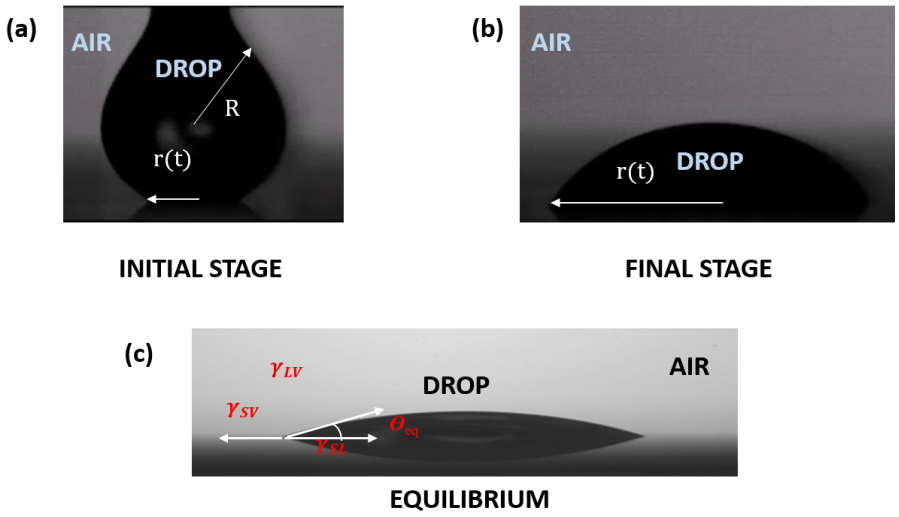

Figure 1.3: (Color online) Schematic of spreading of a liquid drop on a substrate in air. (a) Initial stage of spreading right after the drop makes contact with the substrate. $r(t)$ represents the spreading radius of the drop varying over time. R is the drop radius. (b) Latter (final) stage of spreading, close to equilibrium. (c) Equilibrium configuration of the drop on the substrate. θ_{eq} is the equilibrium contact angle. γ_{SL}, γ_{LV} and γ_{SV} represent the solid-liquid, liquid-vapor and solid-vapor interfacial tensions, respectively.

ing [58, 59], etc. Early works from Voinov [60], Tanner[61] and Cox[62] have shown how viscous dissipation in the vicinity of the three-phase contact line dominates the spreading process close to its equilibrium (see Fig. 1.4b), where the drop contact radius, r grows with time following a scaling [61], $r \sim (\frac{\gamma_{LA} R^9}{\mu_L})^{1/10} t^{1/10}$, where γ_{LA} is the surface tension of liquid drop in air, μ_L is the liquid drop viscosity and R is the drop radius. This particular spreading regime, close to equilibrium, is well understood due to ease of experimentally observing the phenomenon and well established theoretical models. However, the same cannot be said for the initial spreading regime. Just after initial contact, a liquid drop spreads rapidly on a given substrate due to a high curvature of drop-air interface at the moment of contact (see Fig. 1.4a) generating a large interfacial driving force. This initial fast spreading regime lasts only for a few microseconds to a few milliseconds depending on the viscosity of the liq-

uid drop, and hence difficult to observe experimentally. It is also difficult to model analytically due to challenges of infinite curvature of the drop-air interface right at the moment of its contact with the surface. With recent improvements in high-speed imaging techniques and Molecular Dynamic (MD) simulations, the dynamics of this initial fast regime has been investigated in some recent works[63, 64, 65, 66, 67]. In a recent study, Bird et al. showed that for low viscosity drops like water ($\mu_D = 0.001$Pa-s), the initial fast spreading process is dominated by drop inertia with the spreading radius r growing with time following a scaling, $r \sim (\frac{\gamma_{DA}R}{\rho_D})^{1/4} t^{\alpha}$, where the exponent α was found to acquire a value of 1/2 for a completely wetting surface ($\theta_E = 0$) [64]. Further, it was shown that the scaling exponent α changes depending on the wettability of the surface and shows a decreased value of 1/4 for a partially wetting surface with equilibrium contact angle, $\theta_E = 117^{\circ}$ [64]. For their experiments, they observed the spreading process using side-view imaging with a high speed camera. Eddi et al., with a novel bottom view imaging, was able to study the early times of spreading process with improved spatial resolution and found that irrespective of surface wettability, spreading process for high viscosity liquids always began in a regime dominated by drop viscosity and that the process is inherently similar to viscous coalescence of two pendant liquid drops [65]. As far as spreading on an under-liquid surface is concerned, only a handful of literature is available [68, 69, 70, 71]. Goosens et al. studied the spreading of different oil drops on hydrophobic silicon substrates immersed in water and found that the latter, close to equilibrium, spreading regime is dictated by viscous dissipation with linearly additive contribution from both the drop viscosity and surrounding water viscosity [70]. However, their study did not address the initial fast spreading regime in a comprehensive manner [70]. It should be noted that this particular case of spreading considering a surrounding viscous liquid medium is crucial towards the understanding of environmental problems like how pollutant

oil drops wet fish scales[52] and affects other marine lives. The present study aims to contribute towards a comprehensive understanding of this spreading phenomenon on an under-liquid substrate and thereby arrive at a generalized model for spreading of a liquid drop in the presence of another liquid medium.

1.2.3 Wetting on textured surfaces

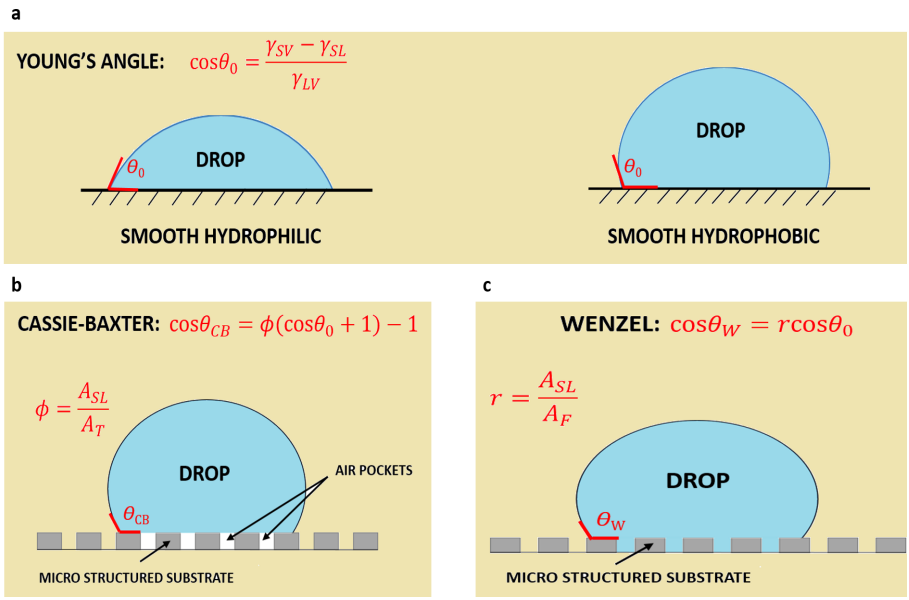

Figure 1.4: (Color online) Wetting on surfaces. (a) Equilibrium configuration of a liquid drop on a smooth hydrophilic and hydrophobic surface. (b) A liquid drop on a textured surface showing the Cassie-Baxter configurations where the liquid drop sits on top of the micro-textures with air trapped beneath. (c) A liquid drop on a textured surface showing the Wenzel configuration with complete penetration of the asperities.

Nature provides ample inspiration for scientific research where behavior such as how raindrops or dew drops interact with a lotus leaf can be effectively mimicked to create similar surfaces with potential applications in real life problems. A lotus leaf with its micro-nano hierarchical structures represents a surface which is hydrophobic, i.e, tendency to repel water drops[6]. Similar to lotus leaves, *taro* leaves have similar textured surface properties which are capable

of demonstrating self-cleaning effects [72]. Further, many insects possess similar micro and nano-scaled, two-tier surface roughness on their wings, which can effectively remove water drops and contaminants [73]. Such hydrophobic textures can be mimicked with standard lithography techniques to create artificial hydrophobic (superhydrophobic) surface with potential applications in self cleaning windows [74, 75, 76], anti-icing [77, 78], surfaces producing low drag in fluid flow[76, 79], surfaces capable of preventing bio-fouling[80, 81], etc. When a liquid drop is deposited on a given textured surface, it either completely penetrates the micro structures exhibiting a Wenzel configuration [82], or it can sit on the top of the micro structures with air trapped beneath, known as the Cassie-Baxter configuration[83] (see Fig. 1.4). For a liquid drop on a textured surface kept in air in a Wenzel configuration, the equilibrium contact angle can be denoted as [82],

$$cos\theta_W = rcos\theta_0 \tag{1.2}$$

where, r is the surface roughness factor defined as the ratio of actual area of solid-liquid interface to the area of solid-liquid interface projected on the horizontal plane and θ_0 is the equilibrium contact angle on the corresponding flat surface, i.e., Young's angle. On the other hand, for the Cassie-Baxter wetting state, the equilibrium contact angle of the drop on the textured surface kept in air can be expressed as [83, 84],

$$cos\theta_{CB} = \phi cos\theta_0 + \phi - 1 \tag{1.3}$$

where, ϕ is the solid-liquid area fraction. Based on the above wetting models, wetting characteristics on such textured surfaces kept in ambient air medium has been widely studied over the last two decades[82, 83, 85, 86, 87, 88, 89, 90, 91, 92, 80, 74, 76, 93, 94]. But what happens when such textured surfaces are kept submerged in water? Are the existing wetting models of Wenzel and Cassie-

Baxter adequate for characterization of textured surfaces under-water? Very few studies have made an attempt to comprehensively answer this question [55, 95, 96, 97, 98]. The relevance of the study can be again found in nature where fish scales and shark skin possess similar micro-nano hierarchical structures which helps them to repel oil drops and under-water pollutants [99]. Such behavior can be mimicked and artificial surfaces can be designed to represent submerged ship parts and under-water pipelines, for drag reduction [76, 99, 79], as well as which can effectively repel oil drops in the event of a marine oil spill [57, 56]. For that purpose, a fundamental understanding of under-liquid wettability of micro-textured surfaces is required. The present work aims to throw some light on this unresolved issue of under-liquid wetting by studying the wetting behavior of oil drops on micro-patterned surfaces kept under-water.

1.3 Thesis organization

This thesis has been organized based on 1 published paper and two papers currently under review in respective peer-reviewed journals. The thesis consists of 5 chapters.

Chapter 1 (the present chapter) serves as the introduction to the thesis and provides the central motivation and objectives of the thesis.

Chapter 2 emphasizes the development of a modified lubrication model to explain the coalescence behavior of two under-liquid sessile drops. A step by step derivation of the governing equation has been shown. The final modified lubrication equation has been analyzed on the basis of significance of each terms present in the equation. The solution methodology and a simplified scaling law has been provided. The coalescence behavior has been explained in terms of growth of liquid bridge height and self-similarity of bridge profile. The effects of viscosity of the drop liquid and surrounding liquid, and the viscosity ratio

therein, on the coalescence process has been analyzed. Relevant conclusions were drawn.

Chapter 3 presents the experimental study of liquid drop spreading on an surface immersed in a second liquid. The experimental technique and has been explained and the results analyzed. The spreading scenarios for different drop liquids in ambient air as well as under-water has been explained thoroughly. A conclusion has been proposed unifying the spreading dynamics of the liquid drops of across a wide range of viscosity on a surface in any given surrounding medium.

Chapter 4 focuses on experimental investigation of behavior of oil drops on an under-liquid micro-patterned surface. The surface fabrication procedure has been briefly explained. The experimental procedure has been stated and results (in terms of contact angle measurements) explained. Special emphasize was given to the receding dynamics of the liquid drop on the micro-patterned substrates placed under-water. The conclusion focused on the discrepancy of experimentally observed values with those predicted by existing theories.

Finally, Chapter 5 summarizes the conclusion drawn from each of the research topics, and briefly discusses future scope.

Bibliography

[1] Pierre-Gilles De Gennes, Françoise Brochard-Wyart, and David Quéré. *Capillarity and wetting phenomena: drops, bubbles, pearls, waves*. Springer Science & Business Media, 2013.

[2] Arthur W Adamson, Alice Petry Gast, et al. Physical chemistry of surfaces. 1967.

[3] Robert D Deegan, Olgica Bakajin, Todd F Dupont, Greb Huber, Sidney R Nagel, and Thomas A Witten. Capillary flow as the cause of ring stains from dried liquid drops. *Nature*, 389(6653):827–829, 1997.

[4] Robert D Deegan, Olgica Bakajin, Todd F Dupont, Greg Huber, Sidney R Nagel, and Thomas A Witten. Contact line deposits in an evaporating drop. *Phy. Rev. E*, 62(1):756, 2000.

[5] John William Strutt and Lord Rayleigh. On the instability of jets. *Proc. London Math. Soc*, 10(4), 1878.

[6] Wilhelm Barthlott and Christoph Neinhuis. Purity of the sacred lotus, or escape from contamination in biological surfaces. *Planta*, 202(1):1–8, 1997.

[7] David L Hu, Brian Chan, and John WM Bush. The hydrodynamics of water strider locomotion. *Nature*, 424(6949):663–666, 2003.

[8] Xuefeng Gao and Lei Jiang. Biophysics: water-repellent legs of water striders. *Nature*, 432(7013):36–36, 2004.

[9] John WM Bush and David L Hu. Walking on water: biolocomotion at the interface. *Annu. Rev. Fluid Mech.*, 38:339–369, 2006.

[10] Pierre-Gilles De Gennes. Wetting: statics and dynamics. *Rev. Mod. Phys.*, 57(3):827, 1985.

[11] Daniel Bonn, Jens Eggers, Joseph Indekeu, Jacques Meunier, and Etienne Rolley. Wetting and spreading. *Rev. Mod. Phys.*, 81(2):739, 2009.

[12] Jens Eggers, John R Lister, and Howard A Stone. Coalescence of liquid drops. *J. Fluid Mech.*, 401:293–310, 1999.

[13] AL Yarin. Drop impact dynamics: splashing, spreading, receding, bouncing. *Annu. Rev. Fluid Mech.*, 38:159–192, 2006.

[14] R Rioboo, M Marengo, and C Tropea. Time evolution of liquid drop impact onto solid, dry surfaces. *Exp. Fluids*, 33(1):112–124, 2002.

[15] Shia-Yen Teh, Robert Lin, Lung-Hsin Hung, and Abraham P Lee. Droplet microfluidics. *Lab Chip*, 8(2):198–220, 2008.

[16] Nasser Ashgriz. *Handbook of atomization and sprays: theory and applications*. Springer Science & Business Media, 2011.

[17] Mira T Guo, Assaf Rotem, John A Heyman, and David A Weitz. Droplet microfluidics for high-throughput biological assays. *Lab Chip*, 12(12):2146–2155, 2012.

[18] XavieráCasadevall i Solvas et al. Droplet microfluidics: recent developments and future applications. *Chem. Commun.*, 47(7):1936–1942, 2011.

[19] EM Freer, T Svitova, and CJ Radke. The role of interfacial rheology in reservoir mixed wettability. *J. Pet. Sci. Eng.*, 39(1):137–158, 2003.

[20] Ronaldo G dos Santos, Rahoma S Mohamed, Antonio C Bannwart, and Watson Loh. Contact angle measurements and wetting behavior of inner surfaces of pipelines exposed to heavy crude oil and water. *J. Pet. Sci. Eng.*, 51(1):9–16, 2006.

[21] Jacob Masliyah, Zhiang Joe Zhou, Zhenghe Xu, Jan Czarnecki, and Hassan Hamza. Understanding water-based bitumen extraction from athabasca oil sands. *Can. J. Chem. Eng.*, 82(4):628–654, 2004.

[22] Naga Siva Kumar Gunda, Bijoyendra Bera, Nikolaos K Karadimitriou, Sushanta K Mitra, and S Majid Hassanizadeh. Reservoir-on-a-chip (roc): a new paradigm in reservoir engineering. *Lab Chip*, 11(22):3785–3792, 2011.

[23] Emanuel Bertrand, Daniel Bonn, Daniel Broseta, H Dobbs, JO Indekeu, J Meunier, K Ragil, and N Shahidzadeh. Wetting of alkanes on water. *J. Pet. Sci. Engg.*, 33(1):217–222, 2002.

[24] Jens Eggers. Theory of drop formation. *Phys. Fluids)*, 7(5):941–953, 1995.

[25] SP Lin and RD Reitz. Drop and spray formation from a liquid jet. *Annu. Rev. Fluid Mech.*, 30(1):85–105, 1998.

[26] Keng-Shiang Huang, Tzung-Heng Lai, and Yu-Cheng Lin. Manipulating the generation of ca-alginate microspheres using microfluidic channels as a carrier of gold nanoparticles. *Lab Chip*, 6(7):954–957, 2006.

[27] Christopher E Sims and Nancy L Allbritton. Analysis of single mammalian cells on-chip. *Lab Chip*, 7(4):423–440, 2007.

[28] Vijay Srinivasan, Vamsee K Pamula, and Richard B Fair. An integrated digital microfluidic lab-on-a-chip for clinical diagnostics on human physiological fluids. *Lab Chip*, 4(4):310–315, 2004.

[29] J Frenkel. Viscous flow of crystalline bodies. *J. Phys. (USSR)*, 16(1):29–38, 1946.

[30] L Duchemin, J Eggers, and C Josserand. Inviscid coalescence of drops. *J. Fluid Mech.*, 487:167–178, 2003.

[31] A Menchaca-Rocha, ANRS Martínez-Dávalos, R Nunez, S Popinet, and S Zaleski. Coalescence of liquid drops by surface tension. *Phys. Rev. E*, 63(4):046309, 2001.

[32] W Yao, HJ Maris, P Pennington, and GM Seidel. Coalescence of viscous liquid drops. *Phys. Rev. E*, 71(1):016309, 2005.

[33] Dirk GAL Aarts, Henk NW Lekkerkerker, Hua Guo, Gerard H Wegdam, and Daniel Bonn. Hydrodynamics of droplet coalescence. *Phys. Rev. Lett.*, 95(16):164503, 2005.

[34] James E Sprittles and Yulii D Shikhmurzaev. A parametric study of the coalescence of liquid drops in a viscous gas. *J. Fluid Mech.*, 753:279–306, 2014.

[35] SP Decent, G Sharpe, AJ Shaw, and PM Suckling. The formation of a liquid bridge during the coalescence of drops. *Int. J. Multiphase Flow*, 32(6):717–738, 2006.

[36] Sarah C Case and Sidney R Nagel. Coalescence in low-viscosity liquids. *Phys. Rev. Lett.*, 100(8):084503, 2008.

[37] James E Sprittles and Yulii D Shikhmurzaev. Dynamics of liquid drops coalescing in the inertial regime. *Phys. Rev. E*, 89(6):063008, 2014.

[38] Joseph D Paulsen. Approach and coalescence of liquid drops in air. *Phys. Rev. E*, 88(6):063010, 2013.

[39] Joseph D Paulsen, Justin C Burton, Sidney R Nagel, Santosh Appathurai, Michael T Harris, and Osman A Basaran. The inexorable resistance of inertia determines the initial regime of drop coalescence. *Proc. Nat. Acad. Sci.*, 109(18):6857–6861, 2012.

[40] Joseph D Paulsen, Rémi Carmigniani, Anerudh Kannan, Justin C Burton, and Sidney R Nagel. Coalescence of bubbles and drops in an outer fluid. *Nat. Comm.*, 5, 2014.

[41] Joseph D Paulsen, Justin C Burton, and Sidney R Nagel. Viscous to inertial crossover in liquid drop coalescence. *Phys. Rev. Lett.*, 106(11):114501, 2011.

[42] WD Ristenpart, PM McCalla, RV Roy, and HA Stone. Coalescence of spreading droplets on a wettable substrate. *Phys. Rev. Lett.*, 97(6):064501, 2006.

[43] JF Hernández-Sánchez, LA Lubbers, Antonin Eddi, and JH Snoeijer. Symmetric and asymmetric coalescence of drops on a substrate. *Phys. Rev. Lett.*, 109(18):184502, 2012.

[44] Nikil Kapur and Philip H Gaskell. Morphology and dynamics of droplet coalescence on a surface. *Phys. Rev. E*, 75(5):056315, 2007.

[45] Min Wook Lee, Dong Kyun Kang, Sam S Yoon, and Alexander L Yarin. Coalescence of two drops on partially wettable substrates. *Langmuir*, 28(8):3791–3798, 2012.

[46] RD Narhe, DA Beysens, and Y Pomeau. Dynamic drying in the early-stage coalescence of droplets sitting on a plate. *Euro. Phys. Lett.*, 81(4):46002, 2008.

[47] Robert W Hopper. Coalescence of two viscous cylinders by capillarity: Part i, theory. *J. Am. Ceram. Soc.*, 76(12):2947–2952, 1993.

[48] Robert W Hopper. Coalescence of two viscous cylinders by capillarity: Part ii, shape evolution. *J. Am. Ceram. Soc.*, 76(12):2953–2960, 1993.

[49] Michael P Brenner, XD Shi, and Sidney R Nagel. Iterated instabilities during droplet fission. *Phys. Rev. Lett.*, 73(25):3391, 1994.

[50] Alexander Oron, Stephen H Davis, and S George Bankoff. Long-scale evolution of thin liquid films. *Rev. Mod. Phys.*, 69(3):931, 1997.

[51] Prashant R Waghmare, Siddhartha Das, and Sushanta K Mitra. Drop deposition on under-liquid low energy surfaces. *Soft Matter*, 9(31):7437–7447, 2013.

[52] Prashant R Waghmare, Naga Siva Kumar Gunda, and Sushanta K Mitra. Under-water superoleophobicity of fish scales. *Sci. Rep.*, 4, 2014.

[53] Edward D Cohen and Edgar B Gutoff. *Modern coating and drying technology*. Jacaranda, 1992.

[54] Hans-Günther Döbereiner, Benjamin Dubin-Thaler, Grégory Giannone, Harry S Xenias, and Michael P Sheetz. Dynamic phase transitions in cell spreading. *Phys. Rev. Lett.*, 93(10):108105, 2004.

[55] Yong Chae Jung and Bharat Bhushan. Wetting behavior of water and oil droplets in three-phase interfaces for hydrophobicity/philicity and oleophobicity/philicity. *Langmuir*, 25(24):14165–14173, 2009.

[56] Bharat Bhushan. Biomimetics inspired surfaces for drag reduction and oleophobicity/philicity. *Beilstein J. Nanotechnol.*, 2(1):66–84, 2011.

[57] Michael Nosonovsky and Bharat Bhushan. Multiscale effects and capillary interactions in functional biomimetic surfaces for energy conversion and green engineering. *Phil. Trans. R. Soc. A*, 367(1893):1511–1539, 2009.

[58] Madhusudan Singh, Hanna M Haverinen, Parul Dhagat, and Ghassan E Jabbour. Inkjet printingprocess and its applications. *Adv. Mater.*, 22(6):673–685, 2010.

[59] Graham D Martin, Stephen D Hoath, and Ian M Hutchings. Inkjet printing-the physics of manipulating liquid jets and drops. In *J. Phys.: Conf. Ser.*, volume 105, page 012001. IOP Publishing, 2008.

[60] OV Voinov. Hydrodynamics of wetting. *Fluid Dyn.*, 11(5):714–721, 1976.

[61] LH Tanner. The spreading of silicone oil drops on horizontal surfaces. *J. Phys. D*, 12(9):1473, 1979.

[62] RG Cox. The dynamics of the spreading of liquids on a solid surface. part 1. viscous flow. *J. Fluid Mech.*, 168:169–194, 1986.

[63] Anne-Laure Biance, Christophe Clanet, and David Quéré. First steps in the spreading of a liquid droplet. *Phys. Rev. E*, 69(1):016301, 2004.

[64] James C Bird, Shreyas Mandre, and Howard A Stone. Short-time dynamics of partial wetting. *Phys. Rev. Lett.*, 100(23):234501, 2008.

[65] Antonin Eddi, Koen G Winkels, and Jacco H Snoeijer. Short time dynamics of viscous drop spreading. *Phys. Fluids*, 25(1):013102, 2013.

[66] Koen G Winkels, Joost H Weijs, Antonin Eddi, and Jacco H Snoeijer. Initial spreading of low-viscosity drops on partially wetting surfaces. *Phys. Rev. E*, 85(5):055301, 2012.

[67] Andreas Carlson, Gabriele Bellani, and Gustav Amberg. Universality in dynamic wetting dominated by contact-line friction. *Phys. Rev. E*, 85(4):045302, 2012.

[68] Melanie Ramiasa, John Ralston, Renate Fetzer, and Rossen Sedev. Contact line friction in liquid–liquid displacement on hydrophobic surfaces. *J. Phys. Chem. C*, 115(50):24975–24986, 2011.

[69] Renate Fetzer, Melanie Ramiasa, and John Ralston. Dynamics of liquid-liquid displacement. *Langmuir*, 25(14):8069–8074, 2009.

[70] Sarah Goossens, David Seveno, Romain Rioboo, Alexandre Vaillant, J Conti, and Joël De Coninck. Can we predict the spreading of a two-liquid system from the spreading of the corresponding liquid–air systems? *Langmuir*, 27(16):9866–9872, 2011.

[71] David Seveno, TD Blake, Sarah Goossens, and Joël De Coninck. Predicting the wetting dynamics of a two-liquid system. *Langmuir*, 27(24):14958–14967, 2011.

[72] Kerstin Koch, Bharat Bhushan, and Wilhelm Barthlott. Diversity of structure, morphology and wetting of plant surfaces. *Soft Matter*, 4(10):1943–1963, 2008.

[73] Doyoung Byun, Jongin Hong, Jin Hwan Ko, Young Jong Lee, Hoon Cheol Park, Bong-Kyu Byun, Jennifer R Lukes, et al. Wetting characteristics of insect wing surfaces. *J. Bionic Eng.*, 6(1):63–70, 2009.

[74] Michael Nosonovsky and Bharat Bhushan. *Multiscale dissipative mechanisms and hierarchical surfaces: friction, superhydrophobicity, and biomimetics*. Springer-Verlag: Heidelberg, Germany, 2008.

[75] Xi Zhang, Feng Shi, Jia Niu, Yugui Jiang, and Zhiqiang Wang. Superhydrophobic surfaces: from structural control to functional application. *J. Mater. Chem.*, 18(6):621–633, 2008.

[76] Bharat Bhushan, Yong Chae Jung, and Kerstin Koch. Micro-, nano-and hierarchical structures for superhydrophobicity, self-cleaning and low adhesion. *Phil. Trans. R. Soc. A*, 367(1894):1631–1672, 2009.

[77] Peng Guo, Yongmei Zheng, Mengxi Wen, Cheng Song, Yucai Lin, and Lei Jiang. Icephobic/anti-icing properties of micro/nanostructured surfaces. *Adv. Mater.*, 24(19):2642–2648, 2012.

[78] Philseok Kim, Tak-Sing Wong, Jack Alvarenga, Michael J Kreder, Wilmer E Adorno-Martinez, and Joanna Aizenberg. Liquid-infused nanostructured surfaces with extreme anti-ice and anti-frost performance. *ACS Nano*, 6(8):6569–6577, 2012.

[79] Samuel Martin and Bharat Bhushan. Modeling and optimization of shark-inspired riblet geometries for low drag applications. *J. Colloid Interface Sci.*, 474:206–215, 2016.

[80] Jan Genzer and Kirill Efimenko. Recent developments in superhydrophobic surfaces and their relevance to marine fouling: a review. *Biofouling*, 22(5):339–360, 2006.

[81] Abraham Marmur. Super-hydrophobicity fundamentals: implications to biofouling prevention. *Biofouling*, 22(02):107–115, 2006.

[82] Robert N Wenzel. Resistance of solid surfaces to wetting by water. *Ind. Eng. Chem.*, 28(8):988–994, 1936.

[83] ABD Cassie and S Baxter. Wettability of porous surfaces. *Trans. Faraday Soc.*, 40:546–551, 1944.

[84] Mathilde Callies and David Quéré. On water repellency. *Soft matter*, 1(1):55–61, 2005.

[85] Christian Dorrer and Jürgen Rühe. Advancing and receding motion of droplets on ultrahydrophobic post surfaces. *Langmuir*, 22(18):7652–7657, 2006.

[86] Glen McHale. Cassie and wenzel: were they really so wrong? *Langmuir*, 23(15):8200–8205, 2007.

[87] Michael Nosonovsky. On the range of applicability of the wenzel and cassie equations. *Langmuir*, 23(19):9919–9920, 2007.

[88] Abraham Marmur. Wetting on hydrophobic rough surfaces: to be heterogeneous or not to be? *Langmuir*, 19(20):8343–8348, 2003.

[89] J Bico, C Tordeux, and D Quéré. Rough wetting. *Europhys. Lett.*, 55(2):214, 2001.

[90] Neelesh A Patankar. Mimicking the lotus effect: influence of double roughness structures and slender pillars. *Langmuir*, 20(19):8209–8213, 2004.

[91] Bharat Bhushan and Yong Chae Jung. Wetting study of patterned surfaces for superhydrophobicity. *Ultramicroscopy*, 107(10):1033–1041, 2007.

[92] Bo He, Neelesh A Patankar, and Junghoon Lee. Multiple equilibrium droplet shapes and design criterion for rough hydrophobic surfaces. *Langmuir*, 19(12):4999–5003, 2003.

[93] Kuan-Yu Yeh, Li-Jen Chen, and Jeng-Yang Chang. Contact angle hysteresis on regular pillar-like hydrophobic surfaces. *Langmuir*, 24(1):245–251, 2008.

[94] Y Kwon, S Choi, N Anantharaju, J Lee, MV Panchagnula, and NA Patankar. Is the cassie- baxter formula relevant? *Langmuir*, 26(22):17528–17531, 2010.

[95] Vahid Hejazi and Michael Nosonovsky. Wetting transitions in two-, three-, and four-phase systems. *Langmuir*, 28(4):2173–2180, 2011.

[96] IE Palamà, S D'Amone, V Arcadio, D Caschera, RG Toro, G Gigli, and B Cortese. Underwater wenzel and cassie oleophobic behaviour. *J. Mater. Chem. A*, 3(7):3854–3861, 2015.

[97] Meihua Jin, Shasha Li, Jing Wang, Zhongxin Xue, Mingyi Liao, and Shutao Wang. Underwater superoleophilicity to superoleophobicity: role of trapped air. *Chem. Commun.*, 48(96):11745–11747, 2012.

[98] Qunfeng Cheng, Mingzhu Li, Yongmei Zheng, Bin Su, Shutao Wang, and Lei Jiang. Janus interface materials: superhydrophobic air/solid interface and superoleophobic water/solid interface inspired by a lotus leaf. *Soft Matter*, 7(13):5948–5951, 2011.

[99] Yunhong Liu and Guangji Li. A new method for producing lotus effect on a biomimetic shark skin. *J. Colloid Interface Sci.*, 388(1):235–242, 2012.

Chapter 2

Symmetric drop coalescence on an under-liquid substrate [1]

2.1 Introduction

Coalescence of two liquid drops kept on an under-liquid substrate is a relevant fluid mechanics problem with potential applications in marine ecosystem, immersion lithography, etc. Even in ambient air, coalescence dynamics of two sessile drops [1, 2, 3, 4, 5] is fundamentally different from that of coalescence of two pendant drops [6, 7, 8, 9, 10, 11, 12, 13, 14, 15, 16, 17, 18] simply due to the challenges posed by the presence of the substrate and therein, the presence of the three-phase contact line. However, from results presented for drop coalescence on substrates kept in air, it was found that the initial coalescence for spreading drops is governed by the bridge geometry and not by the substrate wettability [2]. It is then expected that a surrounding liquid medium would offer significant viscous resistance to the coalescence process and hinder the growth of the liquid bridge connecting the two drops. In doing so, it may significantly

[1] A version of this chapter has been published as : Mitra, S., & Mitra, S. K. (2015). Symmetric drop coalescence on an under-liquid substrate. *Phys. Rev. E*, 92(3), 033013.

alter the initial temporal variation of the bridge height. Similarly, the growth of the bridge width, r_0, i.e, the bridge dimensions in the horizontal plane, may show a different scaling behavior (in air, for viscous drops $r_0 \sim t^{1/2}$ [1]).

In this chapter, a fundamental question pertaining to drop coalescence on an under-liquid substrate, have been addressed: Can a modified version of the one-dimensional lubrication theory be constructed to signify the effect of a surrounding viscous medium and arrive at a unifying framework to understand this problem for any combination of drop and surrounding liquid? Through appropriate theoretical analysis we have formulated a modified one-dimensional lubrication equation to account for the coalescence dynamics, which is valid for a range of viscosity ratios between the liquid drop and the surrounding medium. Further, we have identified the characteristic time scale pertaining to sessile drop coalescence on under-liquid substrates. Our central finding is that there exists a universal scaling regime for bridge height growth both for air and under-liquid substrates for early stage of coalescence. On top of that, it was found that the self similar nature of the bridge profile during the early stage of coalescence persists for lesser time in case of under-liquid substrates as compared to those in air.

2.2 Theory and Formulation

The governing equations for two sessile drops coalescing on a substrate kept immersed in another viscous liquid (see Fig. 2.1) are derived from the creeping flow approximation of the Navier Stokes equation. The drop liquid is considered to be a Newtonian liquid with density ρ_D, viscosity μ_D, moving with a velocity field u_D, and having a pressure field p_D, within a surrounding viscous medium whose viscosity is μ_L. Therefore, the continuity and momentum equations can

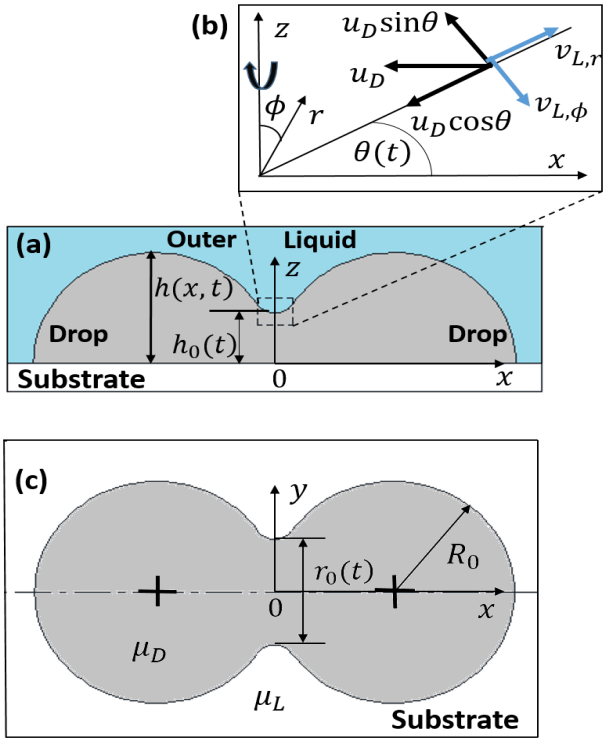

Figure 2.1: (Color online) (a) Side view schematic of the symmetric coalescence process of two equal drops on a substrate in a surrounding viscous medium. $h_0(t)$ indicates the liquid bridge height formed due to the merging drops. (b) The liquid bridge region shown in an extended view representing a symmetric wedge geometry with a wedge angle $\theta(t)$. The velocity vectors are shown at the drop(wedge)-liquid interface. The figure is symmetric about the vertical z-axis. (c) Schematic of the coalescence phenomenon when viewed from top. $r_0(t)$ denotes the bridge growth in the lateral y-direction. R_0 is the original drop base radius.

be written as:

$$\nabla u_D = 0 \tag{2.1}$$

$$\nabla^2 u_D = \nabla p_D \tag{2.2}$$

subjected to boundary conditions: no-slip at the substrate,

$$u_D = 0 : z = 0 \tag{2.3}$$

tangential stress balance at the drop-liquid interface,

$$\tau_L = \tau_D : z = h(x,t) \tag{2.4}$$

and normal stress balance at the drop-liquid interface,

$$p_D = p_L - \gamma \frac{\partial^2 h}{\partial x^2} : z = h(x,t) \tag{2.5}$$

Inherent to such cases where one liquid displaces another one in contact with a surface is a nonintegrable contact line singularity, which is caused by a diverging stress field at the three phase contact line formed by the liquid-liquid-solid system [19, 20]. The common approach to circumvent this challenge is to use an adherence or slip condition near the contact line, as suggested by Huh and Scriven[20]. Another approach to circumvent this problem is to consider the drop profile in the immediate vicinity of the three phase contact line as a liquid wedge [21]. We have taken a similar approach and have considered the drop profiles in the immediate vicinity of the contact line, at the location where the two drops are in contact, as liquid wedges and the surrounding viscous medium essentially gets displaced by sliding up the wedge. In doing so, the slip condition at the contact line has been effectively relieved. When the two drops, originally close to equilibrium, have just made initial contact, the individual wedge an-

gles formed by them with the substrate and surrounding medium will almost be same as their individual equilibrium contact angles. As the drops merge, the wedge angle will gradually diminish over time. It is to be noted here that since we are only considering symmetric coalescence of two equal drops of the same liquid, the wedge angles will be same for both the drop profiles. Further, our analysis is valid for the initial times of coalescence, when the liquid bridge height is much smaller than the overall drop size. The wedge model effectively simplifies the flow model for the surrounding displaced liquid. The two dimensional incompressible flow of the displaced surrounding liquid is modeled using a similar Stokes' equation, but in terms of the stream function, $\psi_L(r,\phi)$. Hence, the governing equation for the flow of the surrounding liquid medium reduces to a bi-harmonic equation with the point of contact of the two liquid wedges as the origin of the polar coordinate system(see Fig. 2.1(b)) and can be expressed as,

$$\nabla^4 \psi_L = 0 \tag{2.6}$$

the solution for which reduces to [20]:

$$\psi_L(r,\phi) = r(asin\phi + bcos\phi + c\phi sin\phi + d\phi cos\phi) \tag{2.7}$$

Upon solution, the velocity components can be expressed as:

$$v_{L,r} = -[acos\phi + bsin\phi + c(sin\phi + \phi cos\phi) + d(cos\phi - \phi sin\phi)] \tag{2.8}$$

$$v_{L,\phi} = asin\phi + bcos\phi + c\phi sin\phi + d\phi cos\phi \tag{2.9}$$

By evaluating the constants a,b,c, and d, and finding $v_{L,r}$ and $v_{L,\phi}$, the stress

balance at the drop-liquid interface can be written as,

$$\mu_D \frac{\partial u_D}{\partial z} = \mu_L \frac{u_D f_1(\theta) + v_{L,0} f_2(\theta)}{z} \tag{2.10}$$

where, $v_{L,0} = \partial h_0/\partial t$ is the velocity of the liquid bridge at $x = 0$, and $f_1(\theta)$ and $f_2(\theta)$ are functions of the gradually diminishing wedge angle, $\theta(t)$. See Appendix A for detailed expressions. From Eqs.[B.1- 2.4, 2.10], the velocity field for the drops can be expressed as:

$$u_D(x,z,t) = \left[\frac{1}{2\mu_D}\left(\frac{\partial p_D}{\partial x}\right) z^2 - \frac{1}{\mu_D}\left(\left(\frac{\partial p_D}{\partial x}\right) h(x,t) + \frac{\mu_L}{h(x,t)} f_2(\theta) v\right) z\right] \times \left[1 - \frac{\mu_L}{\mu_D}\frac{1}{h(x,t)} f_1(\theta) z\right]^{-1} \tag{2.11}$$

Taking into account the pressure exerted by the surrounding liquid on the drops, the drop pressure variation can be found using Eq (5) as:

$$\frac{\partial p_D}{\partial x} = -\rho_L g \frac{\partial h}{\partial x} - \gamma \frac{\partial^3 h}{\partial x^3} \tag{2.12}$$

In the right hand side of Eq.(2.12), the second term representing capillarity makes the dominant contribution. Only when the bridge dimensions are large enough to exceed the capillary length scale of the problem, the hydrostatic pressure head makes significant contribution to the pressure variation. Combining Eqs.[2.11,2.12], we get the expression for the velocity field u_D and hence the the volumetric flow rate, $Q(x,z,t) = \int_0^h u(x,z,t)dz$. On imposing mass conservation, $\frac{\partial h}{\partial t} + \frac{\partial Q}{\partial x} = 0$, the one-dimensional modified lubrication equation for the symmetric drop coalescence on a substrate kept in a surrounding viscous medium can

be expressed as:

$$\frac{\partial h}{\partial t}+\overbrace{\left[\underbrace{\frac{1}{3\mu_D}}_{A1}+\underbrace{\frac{5}{24}\frac{\mu_L}{\mu_D^2}f_1(\theta)}_{B1}+\underbrace{\frac{3}{20}\frac{\mu_L^2}{\mu_D^3}f_1(\theta)^2}_{C1}+...\infty\right]}^{\mu_\infty}\times\frac{\partial}{\partial x}\left(\rho_L g h^3\frac{\partial h}{\partial x}+\gamma h^3\frac{\partial^3 h}{\partial x^3}\right)$$
$$+\frac{\partial h_0}{\partial t}\frac{\partial h}{\partial x}\overbrace{\left[\underbrace{\frac{\mu_L}{\mu_D}f_2(\theta)}_{A2}+\underbrace{\frac{2}{3}\left(\frac{\mu_L}{\mu_D}\right)^2 f_1(\theta)f_2(\theta)}_{B2}+...\infty\right]}^{\mu_{dyn}}=0 \tag{2.13}$$

2.2.1 Analysis of the governing equation

The modified lubrication equation for the symmetric drop coalescence on an under-liquid substrate is valid for an extensive range of viscosity ratios of the drop liquid and surrounding liquid, $\frac{\mu_D}{\mu_L}\sim 10-10^6$. The inverse of the term containing the infinite series in the left-hand side of Eq.(2.13), denoted as μ_∞, represents effective viscosity with contribution from both the drop liquid and surrounding liquid viscosity which is primarily responsible for opposing the capillary attraction between the coalescing drops. The group of terms representing the second infinite series, denoted as μ_{dyn}, reflects effective viscous resistance to the coalescence behavior brought about by the flow in the surrounding viscous liquid. The term A1 (within μ_∞) has the dominant contribution here and only when $\mu_D/\mu_L \leq 200$, each of the other terms B1 , C1 (within μ_∞) and A2 , B2 (within μ_{dyn}) gain prominence. It should be noted here that $f_1(\theta)$ and $f_2(\theta)$ are both negative for a particular drop-liquid combination which clearly signifies that on increasing the surrounding liquid viscosity the duration of the coalescence process will increase. Further, keeping the surrounding liquid viscosity fixed, an increase in drop viscosity also leads to longer coalescence times. On

the other hand, as the viscosity ratio $\frac{\mu_D}{\mu_L}$ increases (i.e., $\frac{\mu_L}{\mu_D}$ becoming smaller), the contribution from the terms B1, C1 and A2, B2 diminishes and for a very large viscosity ratio, such as with air as the surrounding medium, the terms B1, C1, A2 and B2 effectively tend to zero and become negligible. Hence, for such cases, the one-dimensional lubrication equation for drop coalescence in air can be recovered from our modified governing equation[50](See Appendix B for detailed derivation):

$$\frac{\partial h}{\partial t} + \frac{\gamma}{3\mu_D}\frac{\partial}{\partial x}\left(h^3\frac{\partial^3 h}{\partial x^3}\right) = 0 \tag{2.14}$$

For the purpose of scaling analysis, locally in the bridge (i.e., at $x = 0$) the appropriate length scales are $h \sim h_0$ and $\nabla \sim tan\theta_0/h_0$. Using those, the governing equation (Eq. 2.13) locally in the bridge, for early times of coalescence can be expressed as (neglecting gravity),

$$\frac{\partial h_0}{\partial t} + \frac{\gamma tan^4\theta_0}{\mu_{vis}} + \frac{\partial h_0}{\partial t} tan\theta_0\mu_{dyn} = 0 \tag{2.15}$$

where $\mu_{vis} = 1/\mu_\infty$. Hence, the simplified scaling of bridge height growth for early times reduces to,

$$h_0(1 + tan\theta_0\mu_{dyn}) = \frac{\gamma tan^4\theta_0}{\mu_{vis}}t \tag{2.16}$$

On rearranging, the scaling for bridge height growth at early times can be written as,

$$h_0 \sim \frac{\gamma}{\mu_{eff}}t \tag{2.17}$$

where, $\mu_{eff} = \mu_{vis}(1 + tan\theta_0\mu_{dyn})$, represents the effective viscosity dictating the coalescence dynamics.

In a recent study, Ramiasa et al. [22] observed the spreading of oil drops on a

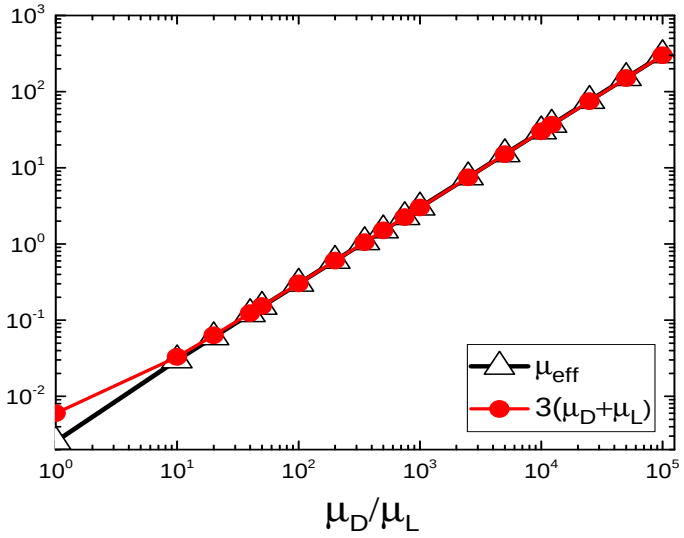

Figure 2.2: (Color online) Comparison of effective viscosity (μ_{eff}) dictating the coalescence process, proposed in this study, (black line, open triangles) with that proposed by Ramiasa et al. [22] (red line, circles)

substrate immersed in water and proposed that the effective viscosity resisting the spreading process is the sum of the drop viscosity and surrounding liquid (water) viscosity, i.e., $\mu_D + \mu_L$. The corresponding effective viscosity resisting the coalescence process studied here can be written as $3(\mu_D + \mu_L)$. On comparing the effective viscosity obtained from the present scaling analysis, i.e., μ_{eff} with that of Ramiasa et al.'s definition of 'effective viscosity', it was found that our proposed representation of the effective viscosity dictating the coalescence process agrees well with the existing theory, as shown in Fig. 2.2. A deviation of our proposed expression from the literature value [68] was observed for drop-surrounding liquid viscosity ratios below 10 (see Fig. 2.2).

2.3 Results and Discussions

An implicit finite difference numerical scheme has been employed to solve the governing equation (Eq.(2.13)) and obtain the temporal evolution of the drop

profile $h(x,t)$. Essentially, the governing equation is discreatized in the x-direction and the resulting ODE is solved using a central difference method. A second order Runge-Kutta technique is employed for the optimal time stepping, where the difference in the obtained profile values between each time step Δt and two half steps $\Delta t/2$ is used for optimal control of the profile shape. For ease of computation, we consider an initial bridge height, h_{00} and the corresponding time elapsed is considered to be t_0. We consider a physical system where laser oil drops of viscosity 0.1Pa-s, 0.2Pa-s, 1Pa-s and 12.2Pa-s are considered as the drop liquid while water ($\mu_L = 0.001$Pa-s) is considered to be the surrounding medium. The drop-surrounding liquid interfacial tension is constant at $33 \times 10^{-3}\mathrm{N \cdot m^{-1}}$ for all the drop viscosity. Each pair of same liquid drops are coalescing on a substrate (with equilibrium contact angle, $\theta_0 = 22^o$) immersed in water. The characteristic viscous length scale ($l_v = {\mu_D}^2/\rho_D\gamma$) for the drops are 2.8×10^{-4}m, 1.14×10^{-3}m, 2.8×10^{-2}m, and 4m, respectively making the creeping flow approximation valid for the initial period of bridge growth (henceforth be called as Regime I). It should be noted that the chosen system yields a wide viscosity ratios of the drop and the surrounding liquid, i.e., $100 \leq \mu_D/\mu_L \leq 12200$.

2.3.1 Varying viscosity of drop and surrounding liquid

The bridge height growth for the early stage of coalescence (Regime I) is shown in Fig. (2.3). It can be seen that the bridge height grows with time following a scaling $h_0 \sim (t - t_0)^{0.89}$ during Regime I of coalescence process. The scaling observed is found to be independent of the viscosity ratio of the two liquids. The largest viscosity ratio shown here is similar to the case when two liquid drops are coalescing in ambient air. It is evident that the scaling observed for Regime I for the present under-liquid coalescence is similar to that observed for coalescence in air medium, i.e., $h_0 \sim t$ [43, 46]. However, it should be noted

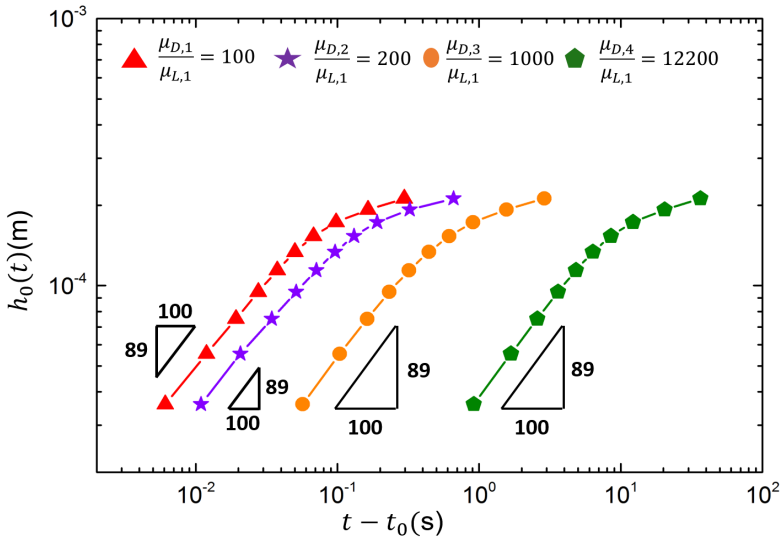

Figure 2.3: (Color online) Growth of the bridge height with time in Regime 1 of coalescence for four different viscosity ratios. For a practical system, it represents laser oil drops of viscosities 0.1 Pa-s, 0.2 Pa-s, 1 Pa-s, and 12.2 Pa-s ($\rho_D = 1100\text{kg}\cdot\text{m}^{-3}$ and $\gamma = 33\times10^{-3}\text{N}\cdot\text{m}^{-1}$), respectively, on a substrate (with equilibrium contact angle $\theta_0 = 22^o$) immersed in water ($\rho_{L,1} = 1000\text{kg}\cdot\text{m}^{-3}$ and $\mu_{L,1} = 1\text{mPa-s}$). Radius of each drop is 1mm so that gravity effects are negligible. The bridge height growth for all cases follows the scaling, $h_0 \sim (t-t_0)^{0.89}$.

that in Fig. 2.3, drops of large viscosity values are used to obtain the different viscosity ratios, while the surrounding liquid viscosity is kept fixed. Hence, it cannot be concluded yet whether the scaling observed is dictated by the viscosity ratio or solely by the drop viscosity. A more comprehensive understanding of the under-liquid coalescence process is required, for which, the role of relatively lower viscosity ratios needs to be taken into consideration. Futher, the effect of variation in the surrounding liquid viscosity needs to be accounted for.

In Figure 2.4a, we have shown the dependance of different viscosity ratios (10, 50 and 100) on the growth of bridge height. In this case, the drop liquid is kept constant and the surrounding liquid is varied, having similar interfacial tension, to obtain the mentioned viscosity ratios. From the curves, it can be seen that on increasing the surrounding liquid viscosity, keeping the drop viscosity constant,

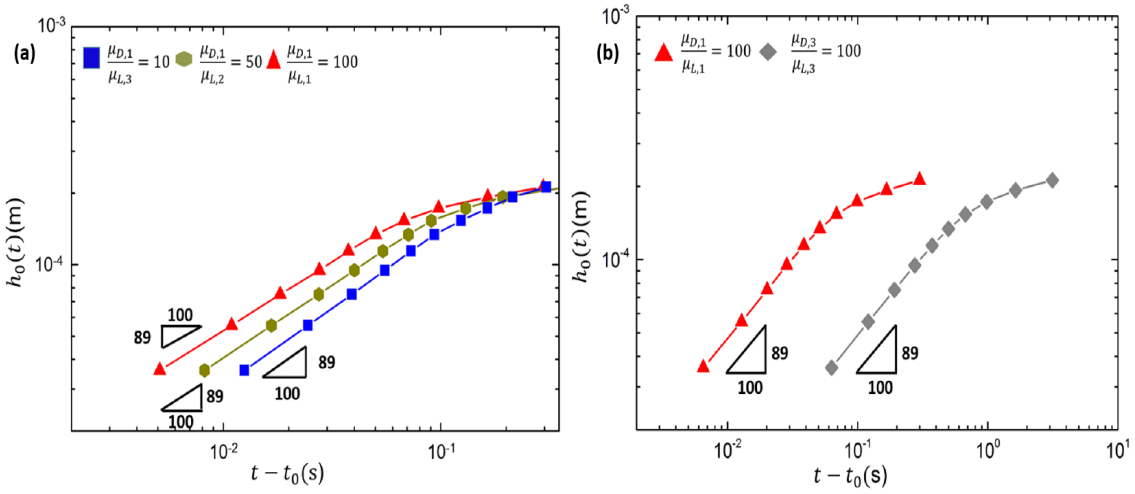

Figure 2.4: (Color online) (a) Growth of the bridge height with time in Regime 1 of coalescence for three different viscosity ratios. In this case, the drop viscosity is kept constant ($\rho_{D,1} = 1100\text{kg}\cdot\text{m}^{-3}, \mu_{D,1} = 0.1\text{Pa-s}$), while the surrounding liquid is varied to obtain viscosity ratios of 10, 50 and 100, having similar interfacial tension of about $33 \times 10^{-3}\text{N}\cdot\text{m}^{-1}$. The bridge height growth for all these cases follows the scaling, $h_0 \sim (t - t_0)^{0.89}$. (b) Evolution of the bridge height versus time in Regime 1 of coalescence for a viscosity ratio of 100. Drops of viscosity 1Pa-s and 0.1Pa-s, respectively, are considered coalescing in the presence of surrounding liquids of viscosity 0.01Pa-s and 0.001Pa-s, respectively to obtain the same viscosity ratio of 100, while interfacial tension is constant at about $33 \times 10^{-3}\text{N}\cdot\text{m}^{-1}$. Here also, the growth of bridge height for all cases was found to obey the scaling, $h_0 \sim (t - t_0)^{0.89}$.

the duration of coalescence increases. However, as observed earlier, the bridge height grows following a similar scaling, $h_0 \sim (t - t_0)^{\alpha}$, where α is 0.89, irrespective of the viscosity ratio. It can be seen from Fig. 2.4a, all the curves merge into a single curve towards the later half of coalescence in Regime I. It can be argued that at this point, the coalescence process undergoes a regime change and enters a regime where the bridge growth slows down, which is referred hereafter as Regime II. Essentially, Regime II signifies a period where the surrounding liquid has been completely displaced out by the coalescing drops. Hence, during this period, it is the drop viscosity that solely dictates the bridge growth dynamics evident from the merging of all the curves. Further, on varying both the drop and surrounding liquid viscosity to arrive at the same viscosity ratio, the same

scaling for the initial period of bridge height growth is observed (see Fig. 2.4b). Upon analysis of all the different cases with appropriate variation of the drop liquid and surrounding liquid viscosity, we arrive at the following conclusions: (a) the coalescence process is primarily dictated by the interfacial tension and the effective viscosity, μ_{eff} and (b) for any viscosity ratio of the drop and surrounding liquid, the bridge height, during early stage of coalescence, grows following a scaling $h_0 \sim t^{\alpha}$, the exponent $\alpha = 0.89$, which is very close to 1, as observed for air [43, 46].

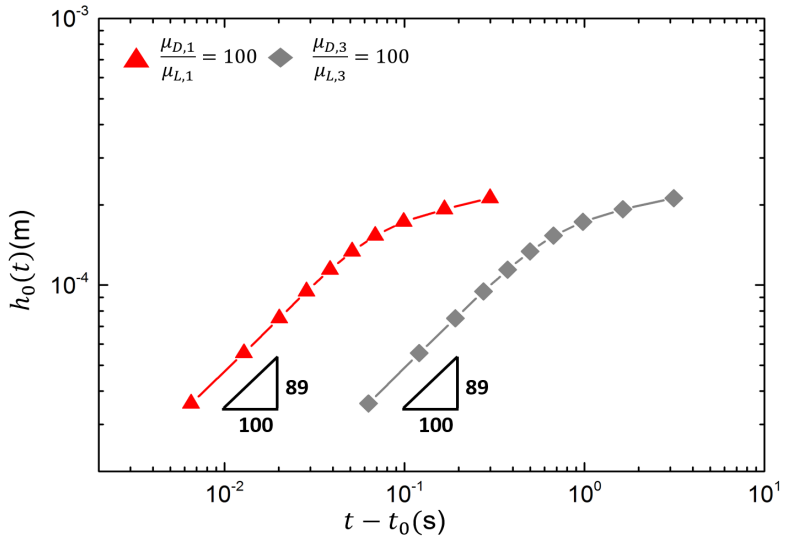

Figure 2.5: (Color online) Growth of the bridge height with time in scaled coordinates. A wide range of viscosity ratios, 10 to 12200 is represented here. For a practical system, it represents any combination of drop and surrounding liquid representing the entire range of viscosity ratios, provided the interfacial tension and the surface wettability remain the same. The solid line shows the bridge height growth with time for symmetric coalescence in air. The dotted lines are the variation for an under-liquid substrate corresponding to Regimes I and II of coalescence, respectively.

2.3.2 Universal scaling behavior

From Eq.2.17, an appropriate characteristic time scale for drop coalescence on an under-liquid substrate can be expressed as,

$$\tau \equiv \frac{\mu_{eff} R_0}{\gamma} \tag{2.18}$$

where R_0 is the drop base radius. On non-dimensionalizing the bridge height as $h^* = h_0/R_0$ and time as $t^* = (t - t_0)/\tau$, it was found that the computed numerical values of bridge height for all the different viscosity ratios collapsed onto a single master curve (Fig. 2.5). From the master curve, it can be concluded that the bridge height scales as $h^* \sim t^{*0.89}$ in the predominant period of initial rapid bridge growth (Regime I) irrespective of the viscosity ratio. Towards later times of coalescence (Regime II), the bridge growth slows down significantly and follows a scaling law, $h^* \sim t^{*0.24}$. Hence, it can be inferred that the bridge height growth at early times of drop coalescence follows a universal behavior.

Further, the growth of the bridge width with respect to time was also studied. From a purely geometrical perspective, the bridge dimensions in perpendicular and lateral directions are related as $r_0 \sim (R_0 h_0/\theta_0)^{1/2}$ [46]. Hence, using the scaling observed for the bridge height with respect to time in presence of the surrounding viscous medium, we arrive at the scaling law followed by the growth of the bridge width, $r^* \sim t^{*0.45}$, in Regime I of the coalescence process(see Fig. 2.6).

2.3.3 Self-similar dynamics

The growth of the liquid bridge during early stage of coalescence (Regime I) follows a self-similar profile, as shown in (Fig.2.7). Essentially, self similarity of bridge profile implies equal growth of the bridge dimensions in horizontal and

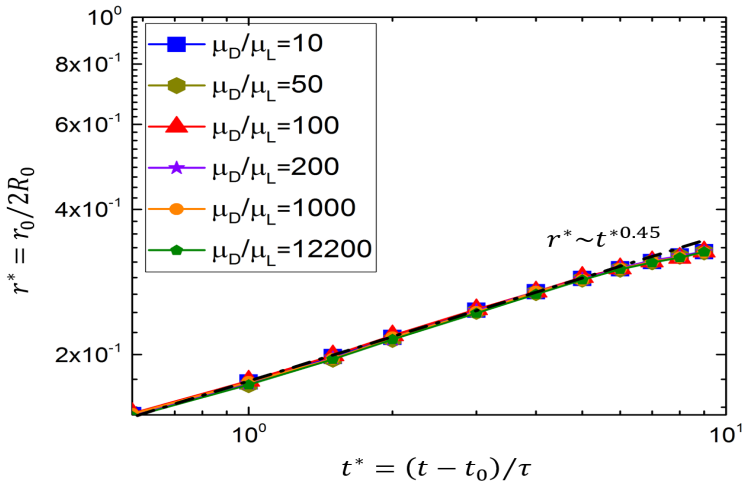

Figure 2.6: (Color online) Growth of the bridge width with respect to time in scaled coordinates for all the different viscosity ratios. The dashed line shows the scaling observed here.

vertical directions. Such self-similarity was shown to exist for drop coalescence in air as well. However, for the present under-liquid case, the self-similarity was observed to persist for a time period much lesser than that observed in air [2]. This can be attributed to the greater viscous resistance to the bridge growth in vertical direction than in the horizontal direction.

2.4 Conclusions

Through appropriate theoretical formulation, a modified lubrication equation is presented to describe the early time coalescence behavior of two sessile drops on an under-liquid substrate. The modified equation adequately accounts for the role of the drop viscosity as well as the surrounding liquid viscosity. It was found that irrespective of the viscosity ratio of the drop and surrounding liquid (even air), the coalescence process initiates in a regime (Regime I) where the liquid bridge height grows linearly with time ($h^* \sim t^*$), thus showing a universal

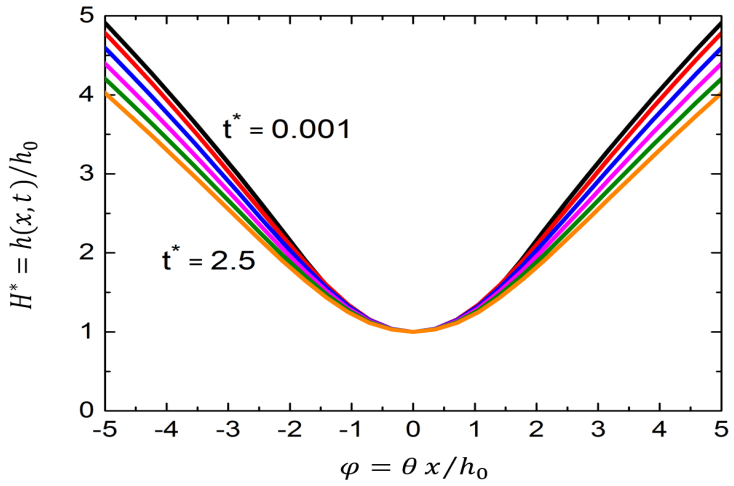

Figure 2.7: (Color online) Bridge profile showing self-similar dynamics for the initial period of bridge growth in Regime I of coalescence ($\mu_D = 0.2$Pa-s, $\mu_L =$ 1mPa-s). The bridge height and position are rescaled as $H^* = h(x,t)/h_0$ and $\varphi = \theta x/h_0$, respectively [43].

behavior. Further, it was found that the coalescence process slows down eventually and enters a regime (Regime II) of slower bridge height growth where the bridge height scales as $h^* \sim t^{*0.24}$. From our numerical analysis, this crossover was observed to occur for $t^* \sim 9$. On extending the scaling behavior of bridge width, presented in Fig. 2.6 to the latter slower regime, solely on the basis of liquid bridge geometry, an exponent of 0.12 was found (i.e., half of the exponent for the bridge height growth). The rate of bridge width growth in Regime II (where the contact line motion begins) is expected to have more dependence on surface wettability. However, at the point of crossover $t^* \sim 9$, the growth rate should retain some dependence on geometry. Interestingly, the exponent 0.12 is very close to that 0.1 exponent commonly seen for drop base radius growth during spreading, as per Tanner's Law [23].

Bibliography

[1] WD Ristenpart, PM McCalla, RV Roy, and HA Stone. Coalescence of spreading droplets on a wettable substrate. *Phys. Rev. Lett.*, 97(6):064501, 2006.

[2] JF Hernández-Sánchez, LA Lubbers, Antonin Eddi, and JH Snoeijer. Symmetric and asymmetric coalescence of drops on a substrate. *Phys. Rev. Lett.*, 109(18):184502, 2012.

[3] Nikil Kapur and Philip H Gaskell. Morphology and dynamics of droplet coalescence on a surface. *Phys. Rev. E*, 75(5):056315, 2007.

[4] Min Wook Lee, Dong Kyun Kang, Sam S Yoon, and Alexander L Yarin. Coalescence of two drops on partially wettable substrates. *Langmuir*, 28(8):3791–3798, 2012.

[5] RD Narhe, DA Beysens, and Y Pomeau. Dynamic drying in the early-stage coalescence of droplets sitting on a plate. *Euro. Phys. Lett.*, 81(4):46002, 2008.

[6] Jens Eggers, John R Lister, and Howard A Stone. Coalescence of liquid drops. *J. Fluid Mech.*, 401:293–310, 1999.

[7] L Duchemin, J Eggers, and C Josserand. Inviscid coalescence of drops. *J. Fluid Mech.*, 487:167–178, 2003.

[8] A Menchaca-Rocha, ANRS Martínez-Dávalos, R Nunez, S Popinet, and S Zaleski. Coalescence of liquid drops by surface tension. *Phys. Rev. E*, 63(4):046309, 2001.

[9] W Yao, HJ Maris, P Pennington, and GM Seidel. Coalescence of viscous liquid drops. *Phys. Rev. E*, 71(1):016309, 2005.

[10] Dirk GAL Aarts, Henk NW Lekkerkerker, Hua Guo, Gerard H Wegdam, and Daniel Bonn. Hydrodynamics of droplet coalescence. *Phys. Rev. Lett.*, 95(16):164503, 2005.

[11] James E Sprittles and Yulii D Shikhmurzaev. A parametric study of the coalescence of liquid drops in a viscous gas. *J. Fluid Mech.*, 753:279–306, 2014.

[12] SP Decent, G Sharpe, AJ Shaw, and PM Suckling. The formation of a liquid bridge during the coalescence of drops. *Int. J. Multiphase Flow*, 32(6):717–738, 2006.

[13] Sarah C Case and Sidney R Nagel. Coalescence in low-viscosity liquids. *Phys. Rev. Lett.*, 100(8):084503, 2008.

[14] James E Sprittles and Yulii D Shikhmurzaev. Dynamics of liquid drops coalescing in the inertial regime. *Phys. Rev. E*, 89(6):063008, 2014.

[15] Joseph D Paulsen. Approach and coalescence of liquid drops in air. *Phys. Rev. E*, 88(6):063010, 2013.

[16] Joseph D Paulsen, Justin C Burton, Sidney R Nagel, Santosh Appathurai, Michael T Harris, and Osman A Basaran. The inexorable resistance of inertia determines the initial regime of drop coalescence. *Proc. Nat. Acad. Sci.*, 109(18):6857–6861, 2012.

[17] Joseph D Paulsen, Rémi Carmigniani, Anerudh Kannan, Justin C Burton, and Sidney R Nagel. Coalescence of bubbles and drops in an outer fluid. *Nat. Comm.*, 5, 2014.

[18] Joseph D Paulsen, Justin C Burton, and Sidney R Nagel. Viscous to inertial crossover in liquid drop coalescence. *Phys. Rev. Lett.*, 106(11):114501, 2011.

[19] Alexander Oron, Stephen H Davis, and S George Bankoff. Long-scale evolution of thin liquid films. *Rev. Mod. Phys.*, 69(3):931, 1997.

[20] Chun Huh and LE Scriven. Hydrodynamic model of steady movement of a solid/liquid/fluid contact line. *J. Colloid Interface Sci.*, 35(1):85–101, 1971.

[21] Pierre-Gilles De Gennes. Wetting: statics and dynamics. *Rev. Mod. Phys.*, 57(3):827, 1985.

[22] Melanie Ramiasa, John Ralston, Renate Fetzer, and Rossen Sedev. Contact line friction in liquid–liquid displacement on hydrophobic surfaces. *J. Phys. Chem. C*, 115(50):24975–24986, 2011.

[23] LH Tanner. The spreading of silicone oil drops on horizontal surfaces. *J. Phys. D*, 12(9):1473, 1979.

[24] Prashant R Waghmare, Siddhartha Das, and Sushanta K Mitra. Drop deposition on under-liquid low energy surfaces. *Soft Matter*, 9(31):7437–7447, 2013.

Chapter 3

How liquid drops spread [1]

3.1 Introduction

Spreading of a liquid drop on a substrate kept submerged in another viscous liquid medium is a relevant problem with manifold applications ranging from oil recovery[1, 2], design of appropriate marine surfaces [3, 4] to droplet microfluidics[5, 6]. The corresponding spreading behavior on a substrate kept in air is well known. For low viscosity liquids like water ($\mu_D = 1$ mPa-s), the spreading process can be characterized as a two stage process: an initial fast spreading regime right after first contact dominated by drop inertia [7, 8, 9, 10, 11] and a latter slower regime, close to equilibrium, dominated by viscous effects [12, 13, 14, 7, 8, 15, 9, 10, 16]. However, for high viscosity liquids like glycerin and viscous mixtures of glycerin and water, the spreading process in air was found to consist of a single viscosity-dominated regime where the drop contact radius grows following a power law, $r \sim t^{\alpha}$, where the apparent exponent α is defined as $\alpha = \frac{d}{d(\log t)}(\log r)$ [15]. It was found that the apparent exponent changes throughout the spreading process from an initial high value of 0.8 to

[1] A version of this chapter has been published as : Mitra, S., & Mitra, S. K. (2016). Understanding the early regime of drop spreading. *Langmuir*, 2016. DOI: 10.1021/acs.langmuir.6b02189, 2016.

a final value of 0.1 close to equilibrium[15]. Further, it was observed that this power law dependence at early times of spreading is inherently similar [15] to the scaling observed for the growth of liquid bridge radius (i.e., $r_b \sim -\frac{1}{\pi} t \log t$) upon coalescence of two pendant drops [17]. The inherent similarity between spreading and coalescence at early times comes from the similar interfacial driving force as well as the self-similar nature of flow profiles [17, 15]. In their recent studies involving coalescence of two pendant drops, Paulsen et al. found that even for low viscosity liquids like water, the coalescence process always begins in a viscosity dominated regime [18, 19, 20]. By the virtue of similarity between spreading and coalescence at early times, it is then expected that spreading too for an extensive range of liquid viscosity can begin in a viscous regime. Despite the theoretical feasibility, experimentally such behavior has not been observed.

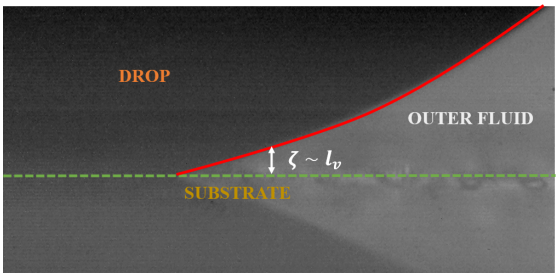

Figure 3.1: (Color online) Initial stage of a liquid drop spreading on a substrate kept in air(or surrounding liquid). The width of the narrow gap ζ is the dominant length scale dictating spreading at this initial stage which scales as the viscous length scale of the problem, l_v.

To better characterize the early time spreading behavior, an important consideration is the characteristic viscous length scale of the process (see Fig. 3.1) denoted by $l_v = \frac{{\mu_D}^2}{\rho_D \gamma_{DA}}$ (where μ_D, ρ_D and γ_{DA} represent drop viscosity, density and surface tension in air, respectively), considering the surrounding medium to be ambient air. We introduce a further parameter to characterize such spreading process in the form of viscosity ratio of drop and the surrounding medium,

μ_D/μ_S, where the surrounding medium can be any gas or liquid. For low viscosity liquids like water ($\mu_D = 1$ mPa-s) drops spreading in air, the viscous length scale is of the order of 20nm and viscosity ratio of the drop and surrounding air (μ_D/μ_S) is 55. Hence, for spreading of water drops on any given surface, even though the spreading process initiates in a viscous regime, it cannot be effectively captured due to limitations in optical diffraction limit coupled with a fast spreading dynamics. Bulk of the literature available has thus been able to study the spreading behavior for such low viscosity liquid drops from an initial inertial regime [7, 8, 9, 10, 11]. On the other hand, for high viscosity liquids like glycerin and silicon oils ($\mu_D \sim 100 - 10^4$ mPa-s), the viscous length scale is of the order of a few millimeters and the corresponding liquid-air viscosity ratio typically can be found in the range of $6000 - 10^5$. Hence, it is logical that the early time spreading process for such liquids remains entirely in a viscous regime [15]. We can further analyze an intermediate class of liquids like dibutyl pthalate and many vegetable oils which has a viscosity of the range 10-50 mPa-s yielding viscosity ratios in the range 550 - 3000 and having characteristic viscous length scale of the order of 10 μm. For such cases, even though an initial viscous regime exists, it is difficult to capture experimentally due to the inherent rapidity of the early time spreading process.

In the present chapter we report the study of this familiar spreading process on an under-liquid substrate. For a substrate immersed in a second viscous medium, the spreading process takes place at a much slower rate than in air. Hence, it is possible to resolve the spatial clarity at very times of spreading. In doing so, it was possible to circumvent all the challenges in terms of spatio-temporal clarity posed by the process in ambient air.

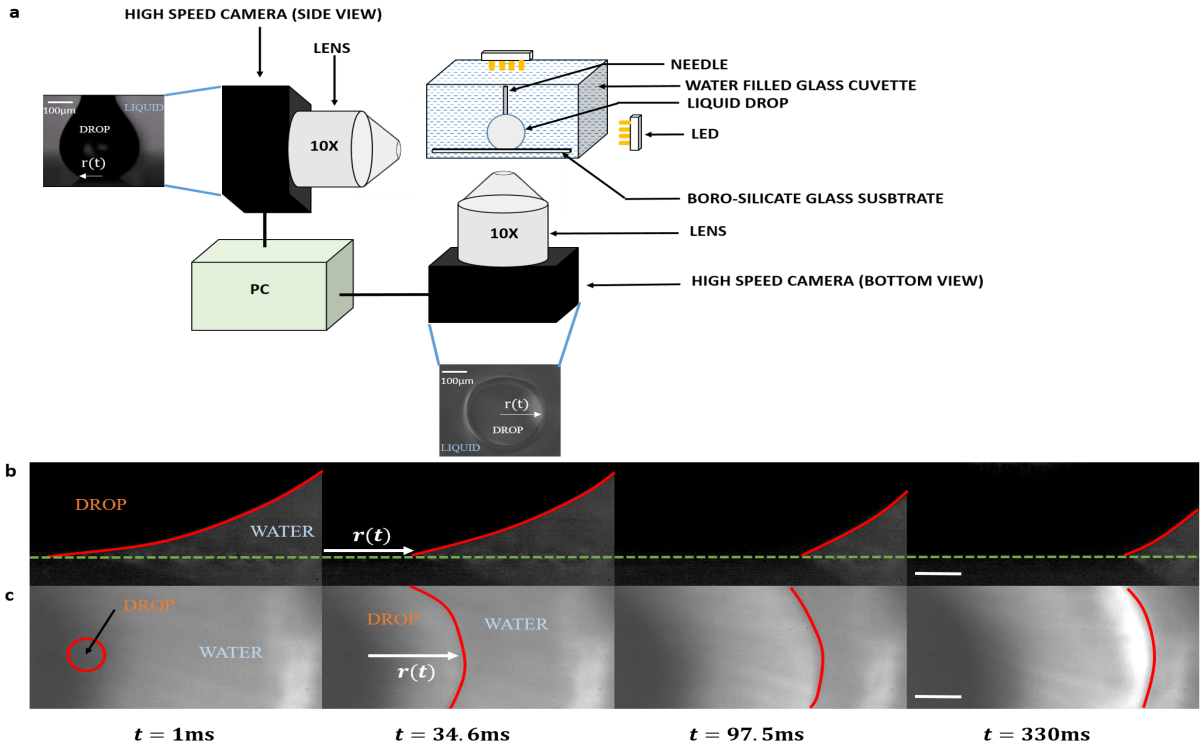

Figure 3.2: (Color online) (a) Experimental set-up of the spreading process. (b) Time snaps obtained from side view imaging, showing the growth of spreading radius r(t) during the spreading of a Dibutyl Pthalate (DBP) drop on a boro-silicate glass substrate kept immersed in a water-filled glass cuvette. The red line indicates the drop-surrounding water interface while the green dotted line represents the substrate location. (c) Corresponding bottom view time snaps. It can be seen that bottom view imaging provides better spatial clarity at very early times (first frame to the left) compared to the respective side view image. The scale bar represents 50μm.

3.2 Experiment

Figure 3.2a shows the experimental set up used for the present study. The spreading behavior of laser oil (Cargille Labs, NJ, USA) and dibuthyl pthalate (DBP) (Sigma-Aldrich, Canada) drops on a boro-silicate glass substrate kept immersed in a water filled glass cuvette (SC-02, Kruss, Germany) was studied. Before each experiment, the glass slides were thoroughly rinsed in ethanol, then sonicated for 10 mins and further cleaned with DI water. A custom-made contact angle measurement system was used to conduct the spreading experiments. A

Table 3.1: Main Physical properties of the liquids used in the experiments

Working Liquids	ρ_D (kg/m^3)	μ_D (mPa-s)	γ_{DA} mN/m	γ_{DW} mN/m	μ_D/μ_A	μ_D/μ_W
Laser oil	1069	200	24.5	33.33	11000	200
DBP	1043	16	31	22	880	16
Water	1000	1	72.1		55	

liquid drop of radius 0.7 mm (so that gravity effects are negligible, See Appendix C) was formed quasi-statically at the tip of a PTFE needle by operating the syring pump at a well defined flow rate of 2-7 μL/min. The drop was then gently made to touch the substrate kept at the bottom of the water-filled glass cuvette to initiate the spreading process. To capture the spreading dynamics, i.e., evolution of the drop contact radius over time, a high speed camera, Photron FASTCAM UX-100 coupled with a 10X optical zoom lens was used. For proper illumination, a cold LED was used. Both side view and bottom view imaging was performed to study the spreading dynamics where bottom view imaging was found to provide better spatial clarity at early times. Figs. 3.2b and 3.2c show the time snaps for the early time spreading behavior obtained from side view and bottom view imaging respectively. To capture the early time spreading process, recording speeds of 8000fps - 10000 fps were used. The recording speeds together with the 10X lens magnification provided a spatial resolution of 1μm/pixel. The captured videos were first broken up into individual frames, which were then analyzed using an image analysis software (ImageJ[21]) to extract the change in spreading radius with time. Each set of experiments were repeated 6 times to ensure consistency. The main uncertainty in the experimental data is in the the spatial resolution for very early times of the drop spreading process where an error corresponding to 1-2 pixels in demarcating the drop-surrounding water interface exists, which translates to an error of 1-2 μm in the measurement of spreading radius.

3.3 Results and Discussions

3.3.1 Spreading under-water

Here, we report the spreading behavior observed for laser and DBP drops on the under-water glass substrate. The spreading process for DBP drops on the under-water glass substrate was observed to initiate in a distinct viscous regime. This is evident from the fact that the growth of spreading radius obeyed a viscous scaling law, $r = C_0 \frac{\gamma_{DW} t}{\pi \mu_D}$, the best fit showing an exponent of 0.95±0.05 (see curve 1 of Fig. 3.3). It should be noted that the prefactor C_0 was found to deviate significantly from unity (the value commonly observed for coalescence of two hanging drops in air [17, 18, 22]). A non-universal prefactor indicates the role of the surrounding liquid viscosity (or the viscosity ratio of the drop and the surrounding liquid, $\mu_D/\mu_W = 16$ in this case). Interestingly, an intermediate regime (see curve 1 of Fig. 3.3) with a distinct power-law growth of $r \sim t^{\alpha}$ was observed right after the initial viscous regime. The exponent α was found to acquire a value of 0.49, i.e., close to 0.5. The power-law growth with an exponent of 0.5 is indicative of a possible inertial regime. However, on comparing with the scaling law normally obsereved for inertial coalescence of two liquid drops in air, i.e., $r = D_0(\frac{\gamma_{DW} R}{\rho_D})^{1/2} t^{1/2}$ it was found that the prefactor D_0 deviated from unity. Hence, in this intermediate regime, as well, a non-universal prefactor was noted indicating the role of the surrounding viscous medium. For liquid drop spreading, the dominant length scale, i.e., the viscous length scale for this process can be characterized by the drop neck height $\zeta \sim l_v \sim \frac{r^2}{2R}$ (see Fig. 3.1) just after the drop makes contact with the substrate[15, 18], where R is the drop radius (0.7mm in our case). Hence, from theory, the critical spreading radius value can be obtained as, $\frac{{r_{C,W}}^2}{2R} = l_v = \frac{{\mu_D}^2}{\rho_D \gamma_{DW}}$. The critical spreading radius effectively denotes a crossover point from a initial viscous to an inertial regime. From

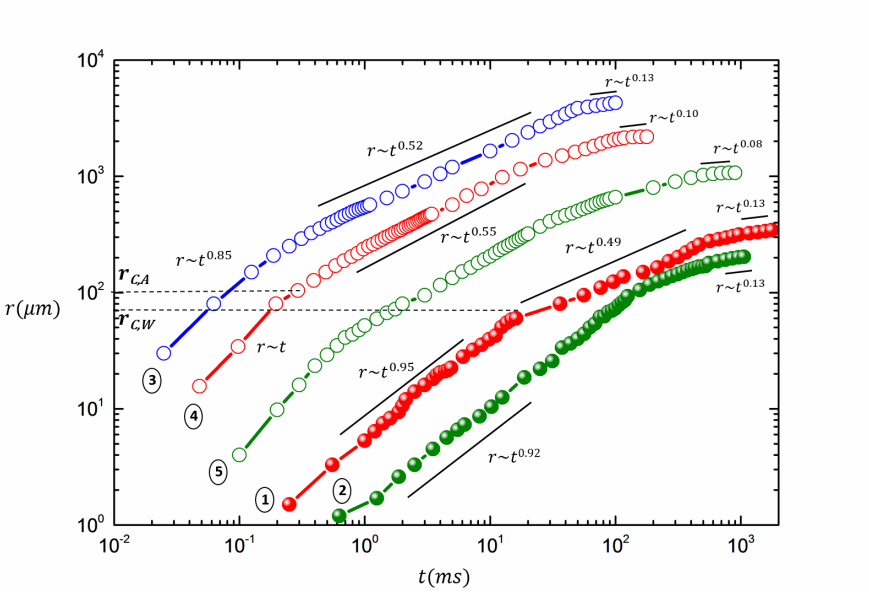

Figure 3.3: (Color online) Curve 1 represents the spreading behavior of DBP drops (R = 0.7mm) on the under-water glass substrate ($\theta_E = 121^\circ$). The initial (viscous) regime shows an exponent of 0.95. A switch to the intermediate (inertial) regime occurs at the critical spreading radius $r_{C,W} = 85\mu$m which conforms to the viscous characteristic length scale of the problem. The spreading of laser oil drops (R=0.7mm) on an under-water glass substrate ($\theta_E = 121^\circ$) is shown in Curve 2. A single initial viscous regime was observed in this case. Curve 3 shows the spreading of DI water drops (R= 1mm) on a glass substrate kept in ambient air. The very early times data indicates a growth of spreading radius with time following a power-law dependence with an exponent 0.85. Following this regime, the inertial regime was observed with an exponent close to 0.5, as indicated. It is to be noted this initial regime matches well with experiments conducted by Biance et al[7]. For DBP drops (R = 1mm) spreading in air (curve 4), a very early regime is observed with a scaling $r \sim t$ (i.e., a viscous regime). Here also, the spreading process switched to an inertial regime corresponding to the critical spreading radius value of $r_{C,A} = 100\mu$m in accordance with the theoretical viscous length scale. The spreading of laser oil on a glass substrate kept in ambient air is shown in Curve 5. The spreading process, in this case, is characterized by a viscous regime in its entirety with a gradually changing scaling exponent (not indicated in the figure). Such a behavior is inherently similar to the variation observed for drop coalescence of high viscosity drops in air[15, 17]). The spreading terminated in the Tanner's regime. $\theta_E < 5^\circ$ for all liquids spreading in air. All the curves terminated in the close to equilibrium viscous regime, i.e., the well known Tanner's regime[14], with an exponent close to 0.1. The error bars are not shown for clarity.

our experimental data, we observe $r_{C,W} = 85\mu$m (corresponding to a 0.7mm radius DBP drop) which matches with the theoretical value (see curve 1 of Fig. 3.3). This confirms that the intermediate regime observed here is an inertial regime with a non-negligible effect of the surrounding liquid viscosity evident from the non-universal prefactor. The spreading process, close to equilibrium followed a scaling law $r \sim t^{0.13}$, i.e., close to Tanner's law [14]. Curve 2 of Fig. 3.3 shows the spreading of laser oil drops on the glass substrate under-water (in this case, $\mu_D/\mu_W = 200$). It can be seen that the spreading process began in a viscous regime, evident from the scaling law for spreading radius growth, $r \sim t$ (best fit exponent of 0.92). Here also, a similar prefactor deviating from unity was observed. However, in this case, no intermediate spreading regime was observed. The spreading process lasted throughout in a viscous dominated regime and culminated in the Tanner's regime[14]. Since the critical spreading radius ($r_{C,W}$) for this case is of the order of a few millimeters, the spreading process always remained in a viscous regime and never switched to an inertial one.

3.3.2 Spreading in air

From our experimental observations of under-liquid spreading, it can be proposed that a spreading process initiating in a viscous regime can be found in liquid-air systems as well where the drop liquid-air viscosity yields a similar ratio. Hence, we revisited the problem from the perspective of spreading of liquid drops on a surface kept in ambient air. Experiments were thus conducted to study the spreading behavior of DBP, laser oil and DI water drops of radius 1mm on the same glass substrate kept in ambient air. Figure 3.4 shows the early time spreading (bottom view images) of the different liquid drops on the boro-silicate glass substrate in air. Water drops spreading in air yields a low viscosity ratio, $\mu_D/\mu_A = 55$. However, it was found that its spreading process began in a regime

where the spreading radius does not show the inertial scaling of $r \sim t^{1/2}$, which should have been the case. Instead, the spreading radius was observed to follow a scaling law, $r \sim t^{0.85}$, i.e., an exponent significantly higher than 0.5 (see curve 3 of Fig 3.3). The duration of this initial regime was only for a period of 0.2ms after initial contact with the substrate before the eventual transition into the familiar inertial regime was observed where the spreading radius grew following a scaling $r \sim t^{1/2}$. This clearly indicates that even for low viscosity drops like water a different spreading regime precedes the conventional inertial one. Existing literature has mostly analyzed spreading behavior of water drops on a substrate kept in ambient air from their experimental data extracted from side-view imaging of the entire process. The inherent problem with side-view imaging, as pointed out by Eddi et al.[15] in their recent study on drop spreading, is poor spatial resolution at early times of spreading. A lack of spatial clarity, therein, makes it difficult to identify the exact moment of contact of the liquid drop with the substrate and thus provides an overestimation of the initial spatial data points. On the other hand, bottom view imaging correctly pin-points the moment of first contact and thus provides early time spatial data with much better accuracy. Our very early time data obtained from bottom view imaging was thus able to identify this different initial spreading regime preceding the commonly seen inertial one. For water drops spreading in air, the critical spreading radius, $r_{C,A}$ is 5μm signifying a transition from the viscous (Stokes) regime to an inertia one. Our observed data for the very early times thus indicates a probable crossover region between the two regimes. The spreading process was observed to culminate in the well known Tanner's regime with a scaling $r \sim t^{1/10}$ (the best fit showed an exponent of 0.13). The spreading of DBP drops in air ($\mu_D/\mu_A = 880$, intermediate) began in a regime where the growth of spreading radius with time was observed to follow a scaling $r = C_1 \frac{\gamma_{DA}}{\pi \mu_D} t$ (curve 4 of Fig. 3.3), with the prefactor C_1 close to unity. In this case, the scaling and prefactor

are identical to that commonly observed for coalescence of two pendant drops of similar viscosity in air[18, 22, 20]. Similar to that observed for water drops spreading in air, the initial viscous regime observed here was only for a short time period due to inherent rapidity of the process. Following the initial viscous regime, the spreading process switches to a distinct second regime where the spreading radius grew following a scaling $r = D_1(\frac{\gamma_{DA}R}{\rho_D})^{1/2}t^{1/2}$ with D_1 of the order of unity. In line with our theoretical prediction, this transition to an inertial regime was observed to occur for a value of spreading radius r_C,A (see curve 4 of Fig. 3.3) which satisfies the condition of viscous characteristic length scale of the problem, ($\zeta \sim l_v = \frac{{r_{C,A}}^2}{2R}$). This confirms that a regime change from an initial viscous dominated Stokes regime to an inertial regime occurs for a spreading radius value which conforms to the viscous characteristic length scale of the problem. At late times of spreading, the Tanner's regime [14] was observed. Finally, for spreading of laser oil drops on glass substrates in air (curve 5 of Fig. 3.3), an entire initial viscous spreading regime was observed with no transition into any inertial regime. Laser oil spreading in air represents a high viscosity ratio ($\mu_D/\mu_A = 11000$) and a viscous characteristic length scale of few millimeters. Hence, a viscous spreading regime in its entirety is obvious. Spreading remained in a viscous dominated regime where the spreading radius scaled as $r \sim t^{\alpha}$, with the apparent exponent α ($0.5 < \alpha < 1.0$) varying throughout the initial regime before finally culminating into the Tanner's regime with a value of 0.08, i.e., close to 0.1. This is similar to the spreading of high viscosity drops in air, as recently observed by Eddi et al.[15].

3.4 Conclusions

Through appropriate experimental and theoretical analysis, we conclude that spreading of sessile drops always begins in a viscous dominated regime irre-

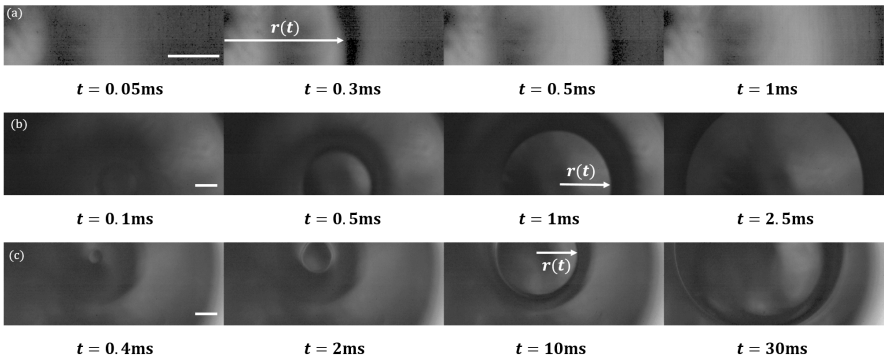

Figure 3.4: (Color online) Time snaps obtained from bottom view imaging of the early time spreading process on the boro-silicate glass substrate kept in air for (a) a 1mm radius water drop (b) a 1mm radius DBP drop and (c) a 1mm radius laser oil drop. r(t) represents the spreading radius growing with time. The scale bar represents 100μm.

spective of the viscosity ratio of the drop and surrounding medium. Further, it was found that for low viscosity ratios, the surrounding medium plays an important role towards the spreading process. This is evident from a non-universal prefactor, which has been previously reported in literature on pendant drop coalescence studies to indicate a non-negligible role of the surrounding medium [15, 17, 18, 24]. Hence, our observed results are in parity with existing literature[15, 17, 18, 24]. In a similar study, Wang et al.[24] observed the coalescence dynamics of water-NaCl drops with oil-tetrachloroethylene mixture as the surrounding medium. They found a prefactor of 0.024, i.e, strongly deviating from unity (commonly seen for coalescence in air), for the initial viscous regime of the liquid bridge growth. This indicates that the prefactor can vary over a wide range and show significant deviation from unity depending on the drop-surrounding liquid combination used. Only when the viscosity ratio reaches the intermediate range, the spreading behavior shows a prefactor of the order of unity. The occurrence of an intermediate inertial spreading regime depends on the viscous length scale of the problem, i.e., the viscous length scale should be of the order which favors a transition from an initial viscous regime to

an inertial one. Only for high viscosity ratios, the Stokes flow for bridge growth rate of two coalescing viscous drops in air with logarithmic corrections accurately describes the spreading picture. For all cases of spreading, the process culminates in the Tanner's regime. Further, it is to be noted here, that DBP and laser oil show equilibrium contact angles of 121° and 134°, respectively, on the glass substrates kept under-liquid i.e., an oleophobic character (any surface which is oleophilic in air almost always exhibits oleophobic nature under-water[23]). But such oleophobicity posed no effect on the scaling exponent observed for their respective spreading dynamics at early times. This substantiates the claim proposed in existing literature[15] about the wettability independent nature of the drop spreading process at early times.

Bibliography

[1] Jacob Masliyah, Zhiang Joe Zhou, Zhenghe Xu, Jan Czarnecki, and Hassan Hamza. Understanding water-based bitumen extraction from athabasca oil sands. *Can. J. Chem. Eng.*, 82(4):628–654, 2004.

[2] EM Freer, T Svitova, and CJ Radke. The role of interfacial rheology in reservoir mixed wettability. *J. Pet. Sci. Eng.*, 39(1):137–158, 2003.

[3] Bharat Bhushan. Biomimetics inspired surfaces for drag reduction and oleophobicity/philicity. *Beilstein J. Nanotechnol.*, 2(1):66–84, 2011.

[4] Yong Chae Jung and Bharat Bhushan. Wetting behavior of water and oil droplets in three-phase interfaces for hydrophobicity/philicity and oleophobicity/philicity. *Langmuir*, 25(24):14165–14173, 2009.

[5] Shia-Yen Teh, Robert Lin, Lung-Hsin Hung, and Abraham P Lee. Droplet microfluidics. *Lab Chip*, 8(2):198–220, 2008.

[6] Joshua D Tice, Helen Song, Adam D Lyon, and Rustem F Ismagilov. Formation of droplets and mixing in multiphase microfluidics at low values of the reynolds and the capillary numbers. *Langmuir*, 19(22):9127–9133, 2003.

[7] Anne-Laure Biance, Christophe Clanet, and David Quéré. First steps in the spreading of a liquid droplet. *Phys. Rev. E*, 69(1):016301, 2004.

[8] James C Bird, Shreyas Mandre, and Howard A Stone. Short-time dynamics of partial wetting. *Phys. Rev. Lett.*, 100(23):234501, 2008.

[9] Koen G Winkels, Joost H Weijs, Antonin Eddi, and Jacco H Snoeijer. Initial spreading of low-viscosity drops on partially wetting surfaces. *Phys. Rev. E*, 85(5):055301, 2012.

[10] Andreas Carlson, Gabriele Bellani, and Gustav Amberg. Universality in dynamic wetting dominated by contact-line friction. *Phys. Rev. E*, 85(4):045302, 2012.

[11] Longquan Chen, Elmar Bonaccurso, and Martin ER Shanahan. Inertial to viscoelastic transition in early drop spreading on soft surfaces. *Langmuir*, 29(6):1893–1898, 2013.

[12] OV Voinov. Hydrodynamics of wetting. *Fluid Dyn.*, 11(5):714–721, 1976.

[13] RG Cox. The dynamics of the spreading of liquids on a solid surface. part 1. viscous flow. *J. Fluid Mech.*, 168:169–194, 1986.

[14] LH Tanner. The spreading of silicone oil drops on horizontal surfaces. *J. Phys. D*, 12(9):1473, 1979.

[15] Antonin Eddi, Koen G Winkels, and Jacco H Snoeijer. Short time dynamics of viscous drop spreading. *Phys. Fluids*, 25(1):013102, 2013.

[16] Michel J De Ruijter, Joël De Coninck, and G Oshanin. Droplet spreading: partial wetting regime revisited. *Langmuir*, 15(6):2209–2216, 1999.

[17] Jens Eggers, John R Lister, and Howard A Stone. Coalescence of liquid drops. *J. Fluid Mech.*, 401:293–310, 1999.

[18] Joseph D Paulsen, Justin C Burton, and Sidney R Nagel. Viscous to inertial crossover in liquid drop coalescence. *Phys. Rev. Lett.*, 106(11):114501, 2011.

[19] Joseph D Paulsen, Justin C Burton, Sidney R Nagel, Santosh Appathurai, Michael T Harris, and Osman A Basaran. The inexorable resistance of inertia determines the initial regime of drop coalescence. *Proc. Nat. Acad. Sci.*, 109(18):6857–6861, 2012.

[20] Joseph D Paulsen, Rémi Carmigniani, Anerudh Kannan, Justin C Burton, and Sidney R Nagel. Coalescence of bubbles and drops in an outer fluid. *Nat. Comm.*, 5, 2014.

[21] Michael D Abràmoff, Paulo J Magalhães, and Sunanda J Ram. Image processing with imagej. *Biophotonics international*, 11(7):36–42, 2004.

[22] Dirk GAL Aarts, Henk NW Lekkerkerker, Hua Guo, Gerard H Wegdam, and Daniel Bonn. Hydrodynamics of droplet coalescence. *Phys. Rev. Lett.*, 95(16):164503, 2005.

[23] Prashant R Waghmare, Siddhartha Das, and Sushanta K Mitra. Underwater superoleophobic glass: Unexplored role of the surfactant-rich solvent. *Sci. Rep.*, 3, 2013.

[24] Luhai Wang, Guifu Zhang, Haiyi Wu, Jiming Yang, and Yujian Zhu. Note: A top-view optical approach for observing the coalescence of liquid drops. *Rev. Sci. Instrum.*, 87(2):026103, 2016.

Chapter 4

Wetting on under-liquid micro-patterned substrates [1]

4.1 Introduction

Surfaces with micro and nano scale hierarchical structures represent a new class of smart surfaces with many real life applications[1, 2, 3, 4, 5, 6, 7]. To study the wetting signature of such a surface in ambient air, the conventional approach is to use the wetting theories proposed by Wenzel [8] and Cassie-Baxter[9]. Indeed, the Wenzel and Cassie-Baxter wetting theories are widely reported to be successful in characterizing the wetting signature of micro-nano textured surfaces in air [1, 7, 3, 10, 11, 12, 13, 14, 15, 16, 17, 18, 19]. However, there has been a recent debate regarding the validity of these two wetting theories [20, 21, 10, 11, 12, 22, 13, 23, 24, 25, 26, 27]. The debate revolves around the fact that these wetting theories are inadequate in characterizing contact angle hysteresis (i.e., the range of contact angles exhibited by a liquid drop on a given rough substrate), which is fundamental towards defining hydrophobicity

[1] A version of this chapter has been submitted as : Mitra, S., Gunda N. S. K., & Mitra, S. K. (2016). Wetting characteristics of under-water micro-patterned surfaces: Is Wenzel and Cassie-Baxter still valid?.*J. Colloid Interface Sci.*, 2016.

(or superhydrophobicity). Further, the theories are based on interfacial area fractions and does not answer questions related to contact line pinning, line tension, etc. Studies by Extrand et al.[22, 25], Gao et al.[20, 26, 27] and many others [28, 29, 30, 31, 32, 33, 34] have echoed this concern and emphasized the fact that interfacial area fractions are not always significant in deciding the wetting configuration of a drop on a rough (heterogeneous or textured) substrate. They pointed out that interaction of the three-phases in the vicinity of the three-phase contact line (i.e., the drop-substrate-air contact line) plays much more significant role in deciding the wetting configuration. In line with that argument many recent studies have proposed alternate wetting models to explain discrepancies between experimentally observed apparent advancing and receding contact angles (i.e., contact angle hysteresis[35]) [22, 23, 30, 31, 32, 33, 36, 37, 38, 39, 40] with those predicted by Wenzel and Cassie-Baxter theories. Further, another critical consideration that needs to be made while studying the wetting behavior on such textured surfaces is the role of energy barrier in Wenzel to Cassie-Baxter transition. Often, a liquid drop on a textured surface prefers to stay in a Cassie-state even though the corresponding Wenzel state is a lower energy state. This is due to the fact that often large free energy barriers separate the two states and for a liquid drop to transition from a Cassie state to a Wenxel state, it effectively needs to overcome the existing free energy barrier [17]. In many cases, the liquid drop fails to overcome that energy barrier and requires some external forcing to make the transition [17, 41, 42]. This implies that multiple static(or equilibrium) states are possible on the same textured surface due to the role of this energy barrier [43, 17]. Wetting transition is indeed a complex issue and only recently some breakthrough has been made to better understand the mechanism of wetting transition on textured surfaces [42, 44, 45, 46, 47, 48, 49, 50, 51]. Such energy barrier can be expressed in terms of a critical pressure [45, 46] below the drop-air interface hanging between two adjacent pillars which ensures

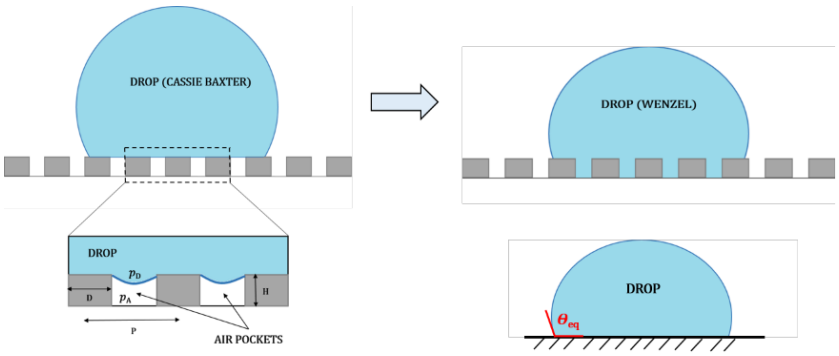

Figure 4.1: (Color online) Schematic of Cassie-Baxter to Wenzel transition of a liquid drop on a micro-patterned substrate (with pillar width D, height H and pitch P) in air. The enlarged view shows the drop-air interface between adjacent pillars. p_D and p_A are the drop and surrounding air pressure, respectively. The configuration of the drop on the corresponding flat substrate (with equilibrium contact angle θ_{eq}) is also shown for reference.

whether the Cassie-Baxter to Wenzel transition is favorable or not (see Fig. 4.1). Mathematically the transition condition in terms of liquid pressure can be expressed as[45, 46]

$$p_D - p_A > -\frac{2\gamma_{DA} cos\theta eq}{(P-D)} \tag{4.1}$$

where, p_D and p_A are the drop and surrounding air pressure, respectively, P and D are the pillar pitch and width (or diameter), respectively, γ_{DA} is the surface tension of liquid drop in air and θ_{eq} is the equilibrium contact angle of the liquid drop on the corresponding flat substrate. If the above condition is satisfied, the drop will transition to a Wenzel state. Otherwise, the drop will be in a (meta)stable Cassie-Baxter state [45, 46].

In this chapter, we aim to check the applicability of Cassie-Baxter and Wenzel theories in characterizing wetting signature for under-liquid micro-patterned surfaces. To achieve this, we have fabricated Silicon based micro-patterned substrates and have studied the wetting behavior of oil drops on such surfaces kept under-water. A comprehensive study has been performed by proper measurement of static, advancing and receding contact angles of oil drops on the micro-patterned surface.

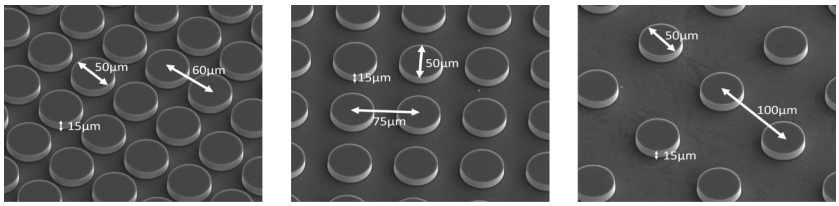

Figure 4.2: SEM micrographs of the Si micro-patterned substrates with the different pillar configurations.

4.2 Experimental Section

4.2.1 Sample Preparation

A 100 mm diameter silicon (Si) substrate (Wafer World Inc., West Palm Beach, FL, USA) was taken as the master surface. Proper cleaning procedure was performed using a standard Piranha solution ($H_2SO_4$and H_2O_2 in 3:1 ratio) and deionised (DI) water, and finally dried under pure nitrogen gas. A positive photoresist (PPR) S1818 (MicroChem Corp, Westborough, MA, USA) was then spin coated at 3000 rpm for 30 seconds followed by soft baking of the coated substrate at 115°C for 60 seconds. The pillars were then patterned on PPR with standard photolithography. Further, the micro-pillars were etched anisotropically on the substrate using deep reactive ion etching (DRIE). After etching, the photoresist was removed in PRS-100 stripper (HTA Enterprises, Microchrome Technology Products, San Jose, CA, USA). The substrates were then cut into $6 \times 6\text{mm}^2$ pieces. The final fabricated substrates consist of arrays of cylindrical micro-pillars constant pillar diameter 50 μm and height 15 μm but varying pitch (60 μm, 75 μm and 100 μm, respectively) (see Fig.4.2). The complete fabrication process flow is available in existing literature[52, 53, 54]. An additional 100 mm-diameter silicon wafer was used and all the chemical treatments, outlined earlier, was performed except the patterning process. Such wafer was also diced into $6 \times 6\text{mm}^2$ pieces, which were then used as standard reference substrates for contact angle measurement.

4.2.2 Instrumentation

The appropriate contact angle measurements were performed in a custom-made contact angle measurement system. The working liquids used were deionized water (density $\rho_W = 1000\text{kg/m}^3$, surface tension in air $\gamma_{WA} = 72.1\text{mN/m}$) and laser oil (Cargille Laboratories Inc., Cedar Grove, NJ, USA; density $\rho_O = 1100\text{kg/m}^3$, surface tension in air $\gamma_{OA} = 24.5\text{mN/m}$). The oil-water interfacial tension, γ_{OW} is 33.33mN/m [51]. Before each experiment, the micro-patterned substrates were thoroughly cleaned with ethanol, sonicated for 10 mins and further cleaned using DI water. The substrates were then dried using nitrogen gas before put to use. The substrates were immersed in a distortion free glass cuvette (Krüss Germany, SC-01) filled with DI water and millimeter sized oil drops were deposited using a microsyringe. Once, the oil drop on the patterned substrate achieve static (or equilibrium) configurations, images were captured using a CCD camera and analyzed using an in-house developed Drop Shape Analysis software to extract the contact angle information. A tangent method [56] was used to measure the contact angle from the observed slope of the three phase contact line associated with each image of the sessile drop. For hysteresis measurements, liquid was pumped into (or out of) an already deposited sessile drop operating the syringe pump at a flow rate of 10μL/min [56]. As the drop volume was increased, the contact angle reached a maximum value close to 180° and on further increase, the three phase contact line shifted to the next pillar. At the instant of this shift, the contact angle was measured from the recorded images, which represents the advancing contact angle, θ_A. Similarly, when liquid was withdrawn from the drop, the receding contact angle, θ_R was measured. Due to the inherent fast advancing and receding dynamics associated with hysteresis, a high speed camera, Photron FASTCAM UX-100 coupled with a 10X zoom lens was used at a frame rate of 50 fps to obtain the accurate visual of the process. For every substrate,

each set of contact angle measurements (advancing, receding and equilibrium) was repeated 5 times to ensure consistency. The contact angles measured were reproducible within an experimental error of $\pm 2^{\circ}$. Contact angle measurements were also conducted on the standard reference flat Si substrates, described earlier, for comparison purpose.

4.3 Results

4.3.1 Static contact angles

Table 4.1: Wenzel roughness factor (R_f) and Cassie fraction (ϕ) for the different micro-patterned substrates used.

pitch (μm)	R_f	ϕ
60	1.6545	0.5454
75	1.4189	0.3491
100	1.2356	0.19625

The equilibrium contact angle, θ_{OW} for an oil drop on a flat surface kept under water can be written as[55],

$$cos\theta_{OW} = \frac{\gamma_{OA} cos\theta_{OA} - \gamma_{WA} cos\theta_{WA}}{\gamma_{OW}} \tag{4.2}$$

where γ_{OA}, γ_{WA} and γ_{OW} are the oil-air, water-air and oil-water interfacial tensions, respectively. $\theta_{OA}$and θ_{WA} are the equilibrium contact angles of oil and water drops on a flat substrate in air, respectively. For wetting on the micro-patterned surfaces, the equilibrium configurations are given by the Wenzel and Cassie-Baxter Equations,

$$cos\theta_W = R_f cos\theta_{eq} \tag{4.3}$$

$$cos\theta_{CB} = R_f \phi cos\theta_{eq} - 1 + \phi \tag{4.4}$$

where $\theta_{eq}(\theta_{OA}, \theta_{WA}, \theta_{OW})$ is the equilibrium contact angle of a liquid drop on the

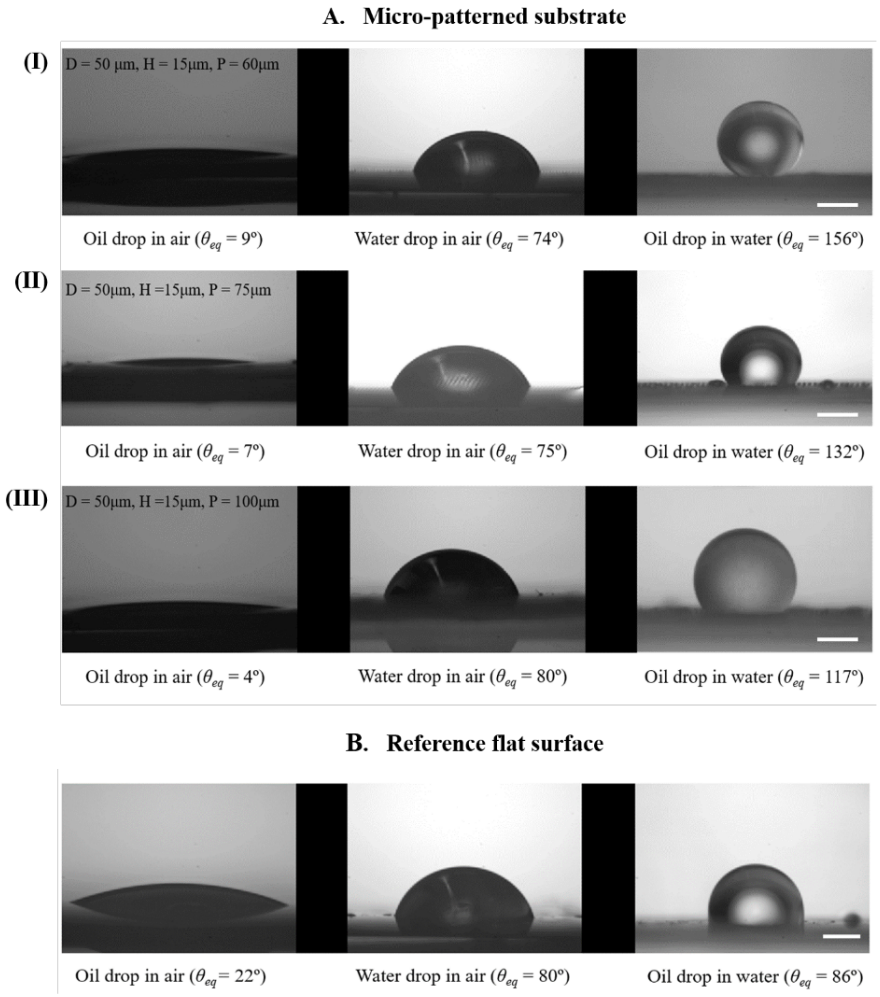

Figure 4.3: A. Static contact angle measurements of oil-Si-air, water-Si-air and oil-Si-water systems for the different micro-patterned silicon substrates: (I) D=50μm, H=15μm, P=60μm, (II) D=50μm, H=15μm, P=75μm and (III) D=50μm, H=15μm, P=100μm. B. Equilibrium configurations of oil-Si-air, water-Si-air and oil-Si-water systems for the reference flat silicon substrate. The scale bar represents 1mm.

flat surface. θ_{OA}, θ_{WA} and θ_{OW} are the equilibrium contact angles for the oil-solid-air, water-solid-air and oil-solid-water systems, respectively. R_f is the roughness factor defined as the ratio of solid-drop liquid contact area to the projection of the solid-liquid contact area on the horizontal plane, and ϕ is the fractional solid-drop liquid contact area. For the micro-patterned substrates used, we consider an unit square cell of cylindrical pillars with diameter D, height H and pitch P.

Then the Wenzel equation reduces to,

$$cos\theta_W = (1 + \frac{\pi DH}{P^2})cos\theta_{eq} \tag{4.5}$$

For the Cassie-Baxter state, the patterned substrates having pillars with smooth tops renders $R_f = 1$. On calculating ϕ, the Cassie-Baxter Equation can be written as,

$$cos\theta_{CB} = \frac{\pi D^2}{4P^2}(cos\theta_{eq} + 1) - 1 \tag{4.6}$$

The static contact angle measurements of oil drops on the different micro-

Table 4.2: Comparison of static contact angles of water drops on the micro-patterned surfaces in air with those predicted by Wenzel configuration (i.e., by computing θ_{Wenzel} from Eq. 4.5 using experimentally observed equilibrium contact angle θ_{WA}).

pitch (μm)	observed equilibrium CA of water in air	theoretical equilibrium CA of water in air
0 (flat)	80° (θ_{WA})	–
60	74°	73°
75	75°	75°
100	80°	77°

patterned substrates as well as the smooth reference substrate is shown in Fig 4.3. The equilibrium configuration of water drops on all the different micro-patterned substrates in air conformed to a Wenzel configuration evident from its contact angle values (see Table 1), while oil drops exhibited very low contact angles (see the first column from the left in Fig. 4.3A) on the substrates in air reminiscent of complete wetting. But in case of wetting of oil drops in under-water configuration, the observed contact angles deviated significantly from those predicted by Wenzel and Cassie-Baxter theories (see Table. 4.3).
It can thus be concluded that as far as static configurations are concerned, the Wenzel (or Cassie Baxter) theory does not accurately capture the wetting dynamics for under-water systems. A mismatch in equilibrium configuration between

Table 4.3: Comparison of static contact angles(CAs) of oil drops on the under-water micro-patterned surfaces with those predicted by Wenzel (Eq. 4.5) and Cassie-Baxter (Eq. 4.6) configurations (i.e., by computing θ_{Wenzel} and θ_{CB} from Eqs. 4.5 and 4.6, respectively, using experimentally observed static contact angle θ_{OW}).

pitch (μm)	observed CA of oil in water	Wenzel CA of oil in water	Cassie-Baxter CA of oil in water
0 (flat)	86° (θ_{OW})	–	–
60	156°	86.6°	115°
75	132°	87°	129°
100	117°	87.5°	142°

our experimental data and existing theory propelled us to perform a hysteresis study to gather more insight into this wetting problem.

4.3.2 Contact angle hysteresis

The focus of the hysteresis study was to see whether the advancing and receding contact angles exhibited by the oil drop on under-water micro-patterned substrates satisfies either the Wenzel or Cassie-Baxter theory. The advancing angles for different micro-patterned surfaces used are shown in Fig. 4.4(i). Imaging under-water is a challenge in itself. The pillars are not completely visible from the raw images (see (a) and (b) of Fig. 4.4(i)). To make the pillar visible significant image analysis was performed whereby the image contrast was improved and better spatial clarity was achieved (see (c) of Fig.4.4(i)). Hence, by proper image correction, the location of the pillars and thereby three-phase contact line (TPCL) was correctly identified. For all the micro-patterned substrates, the advancing contact angles observed were close to 180°. The small difference in the obtained contact angle values is due to difference in image clarity of the individual images which rendered a slightly different fit of the tangent method used. Hence, a slight deviation in the computed contact angle values. Contact angle hysteresis on textured surfaces in ambient air has been widely studied in literature [10, 22, 24, 23, 18, 58] where such high, close to 180°, advancing contact

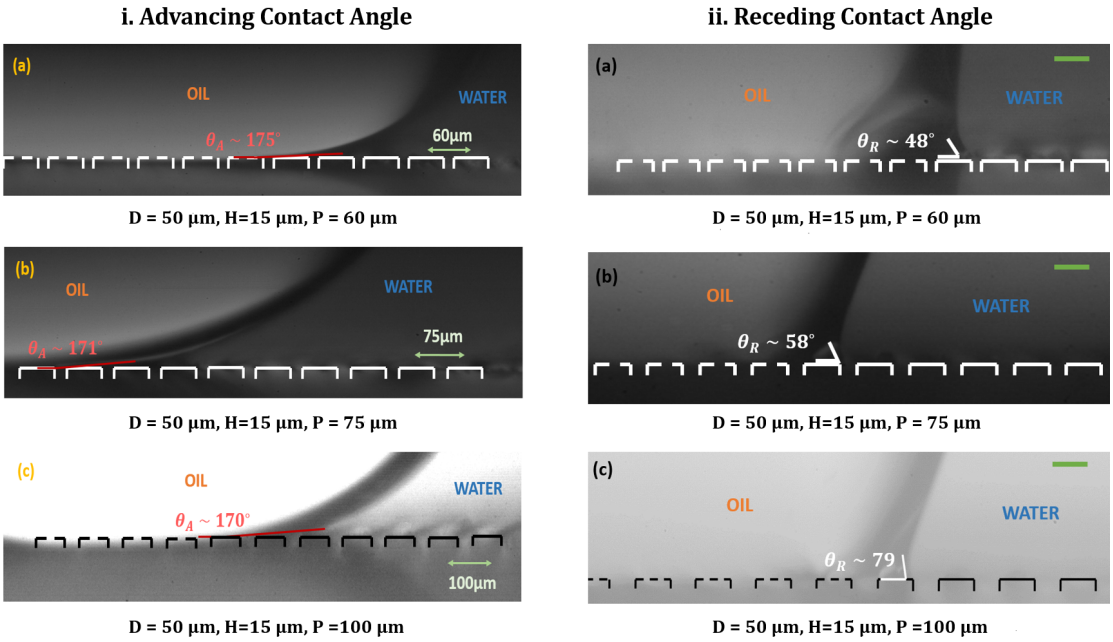

Figure 4.4: (Color online) i. Advancing contact angles of laser oil drops for the different micro-patterned substrates kept under-water: (a) D=50μm, H=15μm, P=60μm, (b) D=50μm, H=15μm, P=75μm and (c) D=50μm, H=15μm, P=100μm. The micro-pillars have been drawn for clarity. It should be noted that the scale bars for (a), (b) and (c) are different as indicated in sub-figures. ii. Receding contact angles of laser oil drops for the different micro-patterned substrates kept under-water:(a) D=50μm, H=15μm, P=60μm, (b) D=50μm, H=15μm, P=75μm and (c) D=50μm, H=15μm, P=100μm. The micro-pillars have been drawn for clarity. The scale bar represents 50μm.

angle has been observed which is parity with our observed results. From a physical interpretation, it is logical for advancing contact angle to achieve a value close to 180°, which is the angle the three-phase contact line needs to reach to touch the next set of pillars while advancing. However, the receding contact angle values showed a wide variation with pillar pitch (see Fig. 4.4 (ii)). The increase in receding contact angles with increasing pillar pitch has also been reported in hysteresis studies in air medium [10, 24, 58]. However, the low receding contact angle values observed here is something new and warrants further investigation.

For a holistic study of under-water wetting behavior of such micro-patterned surfaces, a comprehensive understanding is required in terms of the motion of the

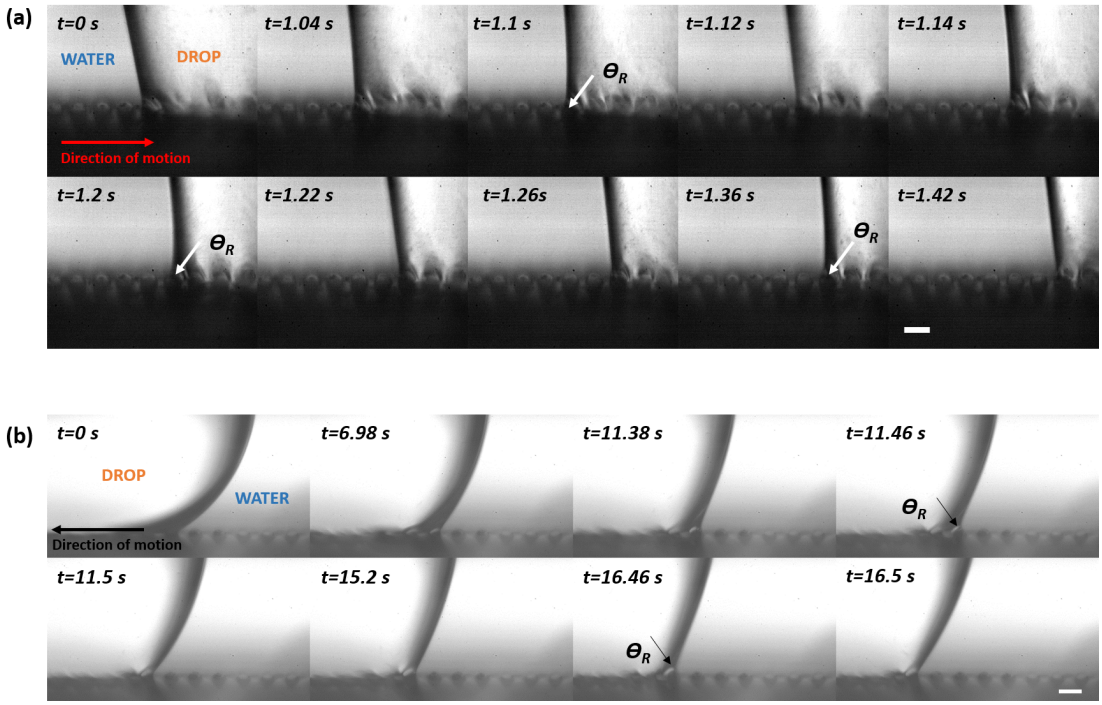

Figure 4.5: (Color online) (a) Time snaps showing the receding mechanism of a laser oil drop on the micro-patterned substrate with pitch 75μm (D= 50μm and H=15 μm) . It can be seen that while receding, the three phase contact line jumped from one pillar top to the adjacent one, one at a time. The frames corresponding to $t = 1.1s$ and $t = 1.36s$ show the three phase contact line just before a jump to the adjacent pillar top and indicates the receding contact angle, $\theta_R = 58^\circ$, in this case. The scale bar represents 100μm. (b) Time snaps showing the receding mechanism of a laser oil drop on the micro-patterned substrate with pitch 100μm (D= 50μm and H=15 μm). Here also, while receding, the three phase contact line jumped from one pillar top to the adjacent one, one at a time. The frames corresponding to $t = 11.46s$ and $t = 16.46s$ show the three phase contact line just before a jump to the adjacent pillar top and indicates the receding contact angle, $\theta_R = 79^\circ$, in this case. The scale bar represents 100μm.

three-phase contact line during advancing and receding motion of the oil drop over the pillars of varying pitch. Hence, we studied the receding mechanism of the oil drop on the substrates in depth. It was found that for the substrate with smallest pillar pitch (i.e., 60μm), the three-phase contact line receded a number of pillars at once when liquid was pumped out of it. On the other hand, for the larger pillar pitches (i.e., 75μm and 100μm) the contact line was observed to shift individual pillar tops while receding (see Figs. 4.5(a) and 4.55(b)). How-

ever, the exact nature of the wetting configuration (Wenzel or Cassie-Baxter) was still unresolved. For under-water systems, a major concern with conventional imaging is a poor visualization of the three phase contact line (TPCL) when it comes to imaging in two axes (x and z, in our case). Such an imaging fails to provide a visualization of the neighboring TPCLs or the drop-water interface between two adjacent TPCLs. Hence, to check whether the oil drop was in a Wenzel or Cassie-Baxter state, it was necessary to modify the imaging technique to have a clear visualization of the receding TPCL as well as the behavior of the neighboring drop-water interface during receding. In that regard, a microscope provides better visualization as far as static drop configuration is concerned. However, for dynamic configurations involving a drop receding, a high speed camera-lens system is a better approach.

To achieve a visualization of the drop receding motion where all the three axes are visible, images were captured by positioning the high speed camera at an angle of about 10° from the reference plane used earlier. Interestingly, it was found that while receding, for patterned substrate with pitch 75μm, locally the drop-water interface is pulled up while the TPCL remained pinned on the adjacent pillar tops (see Fig. 4.6). Then, a single TPCL receded at a time while the neighboring TPCLs remained pinned. Similar phenomenon was also observed for the substrate with pillar pitch 60μm where the contact line was found to recede a number of pillars at once. Hence, the motion was considerably more rapid and could not be captured with high resolution image clarity. The pulling up of the drop-water interface while receding is indicative of a Cassie-like drop configuration since such receding dynamics does not take place for a drop in a Wenzel state. Hence, it can be inferred that the drop configuration is either metastable Cassie-Baxter or an mixed wetting state with partial filling of the protrusions [59].

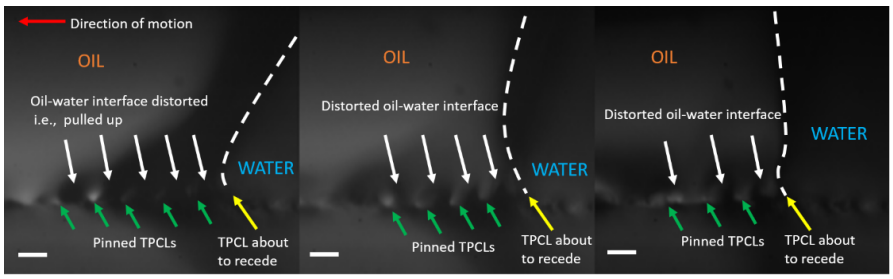

Figure 4.6: (Color online) Receding dynamics observed for an oil drop on an under-water micro-patterned substrate with pillar pitch 75μm when imaged with a slight tilt in camera-lens orientation for the purpose of visualization of the receding mechanism in all the three axes. The pillars, not drawn for this case, are located beneath the three-phase contact lines (TPCLs). When oil is withdrawn from the drop, the oil-water interface connecting two adjacent TPCLs gets pulled up (represented by the white arrows) while the neighboring TPCLs remain pinned on their respective pillar tops (green arrows). The receding motion then takes place with one TPCL receding at a time (yellow arrow) while the neighboring TPCLs remain pinned on their respective pillar tops. The dashed line represents the oil-water interface corresponding to the TPCL which is receding. The scale bar represents 50μm.

4.4 Discussions

4.4.1 Static configuration

The comparison of the experimentally observed advancing and receding contact angles for the different under-water micro-patterned substrates with those predicted by Wenzel and Cassie-Baxter equations is shown in Table. 4.4. The theoretical values are obtained by substituting θ_{eq} with $\theta_{OW,A}$ and $\theta_{OW,R}$ in Eqs. 4.5 and 4.6, where $\theta_{OW,A}$ and $\theta_{OW,R}$ are the experimentally observed advancing and receding contact angles on the corresponding under-water flat reference substrate . Though this approach is debated, still it is widely used in literature to compare expermental values [22, 10, 23, 24, 25, 18, 19]. It was found that other than the receding contact angle for the micro-patterned substrate with pitch 100 μm, none of the advancing and receding angles satisfies Wenzel or Cassie-Baxter theory (see Table 4.4. This further points to the fact that a Wenzel configuration observed in air medium does not always necessarily translate to Wenzel

configuration for under-water systems. For a substrate placed under-water, the surrounding pressure is not merely atmospheric but poses a hydrostatic head, p_H ($\sim \rho_W g h$) brought about by the height h of water column present in the cuvette. Therefore Eq. 4.1, applicable for substrates kept in air, does not hold for the present under-water case. It needs to be modified bringing the account the hydrostatic pressure $\rho_W g h$. Hence, the condition for the critical transition pressure for an under-liquid substrate can be written as:

$$p_D - (p_A + p_H) > -\frac{2\gamma_{OW} cos\theta_{OW}}{(P-D)} \tag{4.7}$$

We argue that the pressure difference across the drop-trapped water interface, $p_D - (p_A + p_H)$ is significantly lower than the corresponding scenario in air, i.e., $p_D - p_A$. Hence, it appears that for the substrates with relatively smaller pitches (i.e., 60μm and 75μm), the critical transition pressure required to make the transition from a Cassie-Baxter to Wenzel state is not reached, making the drop to remain in a Cassie-Baxter or mixed-wetting state. For the substrate with the largest pitch, i.e., 100μm, it appears that the critical transition pressure was achieved and a Wenzel configuration was realized which can be realized from its receding contact angle value. The height of the water column used for the present study is of the order of $\sim 15-18$ mm. Unfortunately, due to constraints posed by our contact angle measurement system, the parameter of liquid column height cannot be varied as an experimental parameter in terms of order of magnitude. The constraints are mostly due to the limitations in vertical needle movement as well as drop size. A more comprehensive computational study of the critical pressure transition criterion would have been helpful in throwing more light into this complex phenomenon of energy barrier mediated wetting configuration. However, such a study is beyond the scope of the present work and can be treated as a topic of future investigation.

Table 4.4: Comparison of advancing and receding contact angles of oil on under-water micro-patterned surfaces with those predicted by Wenzel (Eq.4.5) and Cassie-Baxter (Eq.4.6) configurations (i.e., by computing θ_{Wenzel} and θ_{CB} from Eqs. 4.5 and 4.6, respectively, using experimentally observed advancing and receding contact angles $\theta_{OW,A}$ and $\theta_{OW,R}$).

pitch (μm)	observed advancing and receding CAs θ_A/θ_R	theoretical advancing and receding CAs θ_A/θ_R (Wenzel)	theoretical advancing and receding CAs θ_A/θ_R (CB)
0 (flat)	$103^\circ(\theta_{OW,A})/80^\circ(\theta_{OW,R})$	–	–
60	$175^\circ/48^\circ$	$112^\circ/73^\circ$	$125^\circ/111^\circ$
75	$171^\circ/58^\circ$	$108^\circ/76^\circ$	$136^\circ/126^\circ$
100	$170^\circ/79^\circ$	$106^\circ/78^\circ$	$147^\circ/140^\circ$

4.4.2 Receding contact angle values

From the observation of receding motion, it is evident that wetting configuration of the oil drop on the under-water substrates with pitches 60μm and 75μm is either Cassie-Baxter or mixed wetting state. However, the low receding contact angle values observed on this substrates is something new and puzzling. A low receding contact angle value implies wide contact angle hysteresis (i.e., the difference between advancing and recceding contact angle) which is characteristic of a Wenzel configuration. But, in this case, the results obtained for drop configuration and hysteresis are contradictory. The low receding contact angles observed can be explained from the perspective that often a thin layer of liquid is left behind when the three phase contact line recedes from a particular pillar top. This has been reported by Patankar et al.[21] in a similar study involving contact angle hysteresis on textured surfaces in air. Another possibility can be the formation of precursor film [60, 61]. Formation of such films for under-liquid surfaces is not yet well understood. However, a film formation better explains such low curvature in the vicinity of the three-phase contact line during receding of the drop. The exact interaction of the three phases during drop receding needs to be investigated further in terms of the dynamics of liquid-liquid displacement. In that regard, role of the surrounding medium density and viscosity needs to

emphasized (unlike in ambient air) to arrive at a wetting model to describe such dynamics. Hence, new theoretical studies are required with significant modification to the existing models that hold true for air medium by taking into account the role of the surrounding viscous medium. Also, recent advancement in experimental techniques like laser scanning confocal microscopy[64] would be of great help to understand such under-liquid wetting behavior.

4.5 Conclusion

The present study reports a detailed investigation of wetting characteristics on under-water micro-patterned substrates by studying the interaction of an oil drop with such a under-water substrate. From ou experimental results it can be conclude that the wetting signature (in terms of static, advancing and receding contact angles) cannot be formulated using the existing theoretical models of Wenzel[8] and Cassie-Baxter [9]. Further, the trends seen for wetting on such textured surfaces kept in air medium [1, 7, 3, 10, 11, 12, 13, 14, 15, 16, 17, 18, 19] do not necessarily translate to similar dynamics on surfaces kept under-water. The static drop configuration, which was found to be Wenzel on the substrates kept in air, conformed to a metastable Cassie-Baxter or a mixed wetting state when the same substrates were placed under-water. This is due to the unfavorable free energy barrier that prevented the transition between the wetting states. Further, the drop receding on such an under-water textured substrate showed interesting dynamics. The receding mechanism was found to differ for different pillar pitches. A free energy analysis of the drop-outer liquid-surface system is fundamental towards predicting which configuration (Wenzel, Cassie-Baxter, metastable Cassie-Baxter or a mixed wetting state) is thermodynamically favorable. Also, since the outer liquid liquid is a dense and viscous medium, the dynamics of liquid-liquid displacement needs to be analyzed, particularly how

it dictates the three phase contact line motion in such a system. This understanding is crucial for appropriate characterization of the contact angle with particular emphasize on the receding contact angle. With growing environmental concerns like mitigating the adverse effects of major oil spills (like the recent DeepWater Horizon oil spill event by BP [65]), this basic study on understanding wetting signature of under-water micro-patterned substrates garners relevance in designing appropriate oil repellant and corrosion resistant surfaces. The results presented here points to our lack of complete theoretical understanding of the exact mechanisms that dictate such wetting phenomenon and begs the need to revisit the problem from a comprehensive theoretical viewpoint.

Bibliography

[1] Michael Nosonovsky and Bharat Bhushan. *Multiscale dissipative mechanisms and hierarchical surfaces: friction, superhydrophobicity, and biomimetics*. Springer-Verlag: Heidelberg, Germany, 2008.

[2] Xi Zhang, Feng Shi, Jia Niu, Yugui Jiang, and Zhiqiang Wang. Superhydrophobic surfaces: from structural control to functional application. *J. Mater. Chem.*, 18(6):621–633, 2008.

[3] Bharat Bhushan, Yong Chae Jung, and Kerstin Koch. Micro-, nano-and hierarchical structures for superhydrophobicity, self-cleaning and low adhesion. *Phil. Trans. R. Soc. A*, 367(1894):1631–1672, 2009.

[4] Peng Guo, Yongmei Zheng, Mengxi Wen, Cheng Song, Yucai Lin, and Lei Jiang. Icephobic/anti-icing properties of micro/nanostructured surfaces. *Adv. Mater.*, 24(19):2642–2648, 2012.

[5] Philseok Kim, Tak-Sing Wong, Jack Alvarenga, Michael J Kreder, Wilmer E Adorno-Martinez, and Joanna Aizenberg. Liquid-infused nanostructured surfaces with extreme anti-ice and anti-frost performance. *ACS Nano*, 6(8):6569–6577, 2012.

[6] Samuel Martin and Bharat Bhushan. Modeling and optimization of shark-inspired riblet geometries for low drag applications. *J. Colloid Interface Sci.*, 474:206–215, 2016.

[7] Jan Genzer and Kirill Efimenko. Recent developments in superhydrophobic surfaces and their relevance to marine fouling: a review. *Biofouling*, 22(5):339–360, 2006.

[8] Robert N Wenzel. Resistance of solid surfaces to wetting by water. *Ind. Eng. Chem.*, 28(8):988–994, 1936.

[9] ABD Cassie and S Baxter. Wettability of porous surfaces. *Trans. Faraday Soc.*, 40:546–551, 1944.

[10] Christian Dorrer and Jürgen Rühe. Advancing and receding motion of droplets on ultrahydrophobic post surfaces. *Langmuir*, 22(18):7652–7657, 2006.

[11] Glen McHale. Cassie and wenzel: were they really so wrong? *Langmuir*, 23(15):8200–8205, 2007.

[12] Michael Nosonovsky. On the range of applicability of the wenzel and cassie equations. *Langmuir*, 23(19):9919–9920, 2007.

[13] Abraham Marmur. Wetting on hydrophobic rough surfaces: to be heterogeneous or not to be? *Langmuir*, 19(20):8343–8348, 2003.

[14] J Bico, C Tordeux, and D Quéré. Rough wetting. *Europhys. Lett.*, 55(2):214, 2001.

[15] Neelesh A Patankar. Mimicking the lotus effect: influence of double roughness structures and slender pillars. *Langmuir*, 20(19):8209–8213, 2004.

[16] Bharat Bhushan and Yong Chae Jung. Wetting study of patterned surfaces for superhydrophobicity. *Ultramicroscopy*, 107(10):1033–1041, 2007.

[17] Bo He, Neelesh A Patankar, and Junghoon Lee. Multiple equilibrium droplet shapes and design criterion for rough hydrophobic surfaces. *Langmuir*, 19(12):4999–5003, 2003.

[18] Kuan-Yu Yeh, Li-Jen Chen, and Jeng-Yang Chang. Contact angle hysteresis on regular pillar-like hydrophobic surfaces. *Langmuir*, 24(1):245–251, 2008.

[19] Y Kwon, S Choi, N Anantharaju, J Lee, MV Panchagnula, and NA Patankar. Is the cassie- baxter formula relevant? *Langmuir*, 26(22):17528–17531, 2010.

[20] Lichao Gao and Thomas J McCarthy. How wenzel and cassie were wrong. *Langmuir*, 23(7):3762–3765, 2007.

[21] Neelesh A Patankar. On the modeling of hydrophobic contact angles on rough surfaces. *Langmuir*, 19(4):1249–1253, 2003.

[22] CW Extrand. Model for contact angles and hysteresis on rough and ultraphobic surfaces. *Langmuir*, 18(21):7991–7999, 2002.

[23] Craig Priest, Trent WJ Albrecht, Rossen Sedev, and John Ralston. Asymmetric wetting hysteresis on hydrophobic microstructured surfaces. *Langmuir*, 25(10):5655–5660, 2009.

[24] Didem Öner and Thomas J McCarthy. Ultrahydrophobic surfaces. effects of topography length scales on wettability. *Langmuir*, 16(20):7777–7782, 2000.

[25] CW Extrand. Contact angles and hysteresis on surfaces with chemically heterogeneous islands. *Langmuir*, 19(9):3793–3796, 2003.

[26] Lichao Gao and Thomas J McCarthy. Reply to comment on how wenzel and cassie were wrong by gao and mccarthy. *Langmuir*, 23(26):13243–13243, 2007.

[27] Lichao Gao and Thomas J McCarthy. Wetting 101. *Langmuir*, 25(24):14105–14115, 2009.

[28] FE Bartell and JW Shepard. Surface roughness as related to hysteresis of contact angles. ii. the systems paraffin–3 molar calcium chloride solution–air and paraffin–glycerol–air. *J. Phys. Chem.*, 57(4):455–458, 1953.

[29] JF Joanny and Pierre-Gilles De Gennes. A model for contact angle hysteresis. *J. Chem. Phys.*, 81(1):552–562, 1984.

[30] Wonjae Choi, Anish Tuteja, Joseph M Mabry, Robert E Cohen, and Gareth H McKinley. A modified cassie–baxter relationship to explain contact angle hysteresis and anisotropy on non-wetting textured surfaces. *J. Colloid Interface Sci.*, 339(1):208–216, 2009.

[31] Neeharika Anantharaju, Mahesh V Panchagnula, Srikanth Vedantam, Sudhakar Neti, and Svetlana Tatic-Lucic. Effect of three-phase contact line topology on dynamic contact angles on heterogeneous surfaces. *Langmuir*, 23(23):11673–11676, 2007.

[32] Rishi Raj, Ryan Enright, Yangying Zhu, Solomon Adera, and Evelyn N Wang. Unified model for contact angle hysteresis on heterogeneous and superhydrophobic surfaces. *Langmuir*, 28(45):15777–15788, 2012.

[33] Simon Tylsgaard Larsen and Rafael Taboryski. A cassie-like law using triple phase boundary line fractions for faceted droplets on chemically heterogeneous surfaces. *Langmuir*, 25(3):1282–1284, 2009.

[34] Anaïs Gauthier, Marco Rivetti, Jérémie Teisseire, and Etienne Barthel. Role of kinks in the dynamics of contact lines receding on superhydrophobic surfaces. *Phys. Rev. Lett.*, 110(4):046101, 2013.

[35] W Li and A Amirfazli. A thermodynamic approach for determining the contact angle hysteresis for superhydrophobic surfaces. *J. Colloid Interface Sci.*, 292(1):195–201, 2005.

[36] Tingyi Leo Liu, Zhiyu Chen, and Chang-Jin Kim. A dynamic cassie–baxter model. *Soft Matter*, 11(8):1589–1596, 2015.

[37] Ashutosh Shastry, Shaghayegh Abbasi, Aziel Epilepsia, and Karl F Bohringer. Contact angle hysteresis characterization of textured superhydrophobic surfaces. In *in International Solid-State Sensors, Actuators and Microsystems Conference (Transducers'07)*, pages 599–602. IEEE, 2007.

[38] Renaud Dufour, Maxime Harnois, Vincent Thomy, Rabah Boukherroub, and Vincent Senez. Contact angle hysteresis origins: Investigation on super-omniphobic surfaces. *Soft Matter*, 7(19):9380–9387, 2011.

[39] Tianzhun Wu and Yuji Suzuki. Design, microfabrication and evaluation of robust high-performance superlyophobic surfaces. *Sens. Actuators, B*, 156(1):401–409, 2011.

[40] Edward Bormashenko. General equation describing wetting of rough surfaces. *J. Colloid Interface Sci.*, 360(1):317–319, 2011.

[41] José Bico, Christian Marzolin, and David Quéré. Pearl drops. *Europhys. Lett.*, 47(2):220, 1999.

[42] Zen Yoshimitsu, Akira Nakajima, Toshiya Watanabe, and Kazuhito Hashimoto. Effects of surface structure on the hydrophobicity and sliding behavior of water droplets. *Langmuir*, 18(15):5818–5822, 2002.

[43] Rulon E Johnson Jr and Robert H Dettre. Contact angle hysteresis. iii. study of an idealized heterogeneous surface. *J. Phys. Chem.*, 68(7):1744–1750, 1964.

[44] Pontus Forsberg, Fredrik Nikolajeff, and Mikael Karlsson. Cassie–wenzel and wenzel–cassie transitions on immersed superhydrophobic surfaces under hydrostatic pressure. *Soft Matter*, 7(1):104–109, 2011.

[45] Neelesh A Patankar. Consolidation of hydrophobic transition criteria by using an approximate energy minimization approach. *Langmuir*, 26(11):8941–8945, 2010.

[46] Alberto Giacomello, Mauro Chinappi, Simone Meloni, and Carlo Massimo Casciola. Metastable wetting on superhydrophobic surfaces: continuum and atomistic views of the cassie-baxter–wenzel transition. *Phys. Rev. Lett.*, 109(22):226102, 2012.

[47] Q-S Zheng, Yang Yu, and Z-H Zhao. Effects of hydraulic pressure on the stability and transition of wetting modes of superhydrophobic surfaces. *Langmuir*, 21(26):12207–12212, 2005.

[48] H Kusumaatmaja, ML Blow, AVJM Dupuis, and JM Yeomans. The collapse transition on superhydrophobic surfaces. *Europhys. Lett.*, 81(3):36003, 2008.

[49] Edward Bormashenko. Wetting transitions on biomimetic surfaces. *Phil. Trans. R. Soc. A*, 368(1929):4695–4711, 2010.

[50] Biao Liu and Fred F Lange. Pressure induced transition between superhydrophobic states: configuration diagrams and effect of surface feature size. *J. Colloid Interface Sci.*, 298(2):899–909, 2006.

[51] Edward Bormashenko. Progress in understanding wetting transitions on rough surfaces. *Adv. Colloid Interface Sci.*, 222:92–103, 2015.

[52] Naga Siva Kumar Gunda, Minashree Singh, Yashasvi Purwar, Sirish L Shah, Kamaljit Kaur, and Sushanta K Mitra. Micro-spot with integrated pillars (msip) for detection of dengue virus ns1. *Biomed. Microdevices*, 15(6):959–971, 2013.

[53] Naga Siva Kumar Gunda, Jerry Joseph, Ali Tamayol, Mohsen Akbari, and Sushanta K Mitra. Measurement of pressure drop and flow resistance in microchannels with integrated micropillars. *Microfluid. Nanofluid.*, 14(3-4):711–721, 2013.

[54] Naga Siva Kumar Gunda, Bijoyendra Bera, Nikolaos K Karadimitriou, Sushanta K Mitra, and S Majid Hassanizadeh. Reservoir-on-a-chip (roc): a new paradigm in reservoir engineering. *Lab Chip*, 11(22):3785–3792, 2011.

[55] Prashant R Waghmare, Siddhartha Das, and Sushanta K Mitra. Drop deposition on under-liquid low energy surfaces. *Soft Matter*, 9(31):7437–7447, 2013.

[56] Prashant R Waghmare and Sushanta K Mitra. Contact angle hysteresis of microbead suspensions. *Langmuir*, 26(22):17082–17089, 2010.

[57] Yong Chae Jung and Bharat Bhushan. Wetting behavior of water and oil droplets in three-phase interfaces for hydrophobicity/philicity and oleophobicity/philicity. *Langmuir*, 25(24):14165–14173, 2009.

[58] H Kusumaatmaja and JM Yeomans. Modeling contact angle hysteresis on chemically patterned and superhydrophobic surfaces. *Langmuir*, 23(11):6019–6032, 2007.

[59] Samira Farsinezhad, Prashant R Waghmare, Benjamin D Wiltshire, Himani Sharma, Saeid Amiri, Sushanta K Mitra, and Karthik Shankar. Amphiphobic surfaces from functionalized tio 2 nanotube arrays. *RSC Adv.*, 4(63):33587–33598, 2014.

[60] Pierre-Gilles De Gennes. Wetting: statics and dynamics. *Rev. Mod. Phys.*, 57(3):827, 1985.

[61] Daniel Bonn, Jens Eggers, Joseph Indekeu, Jacques Meunier, and Etienne Rolley. Wetting and spreading. *Rev. Mod. Phys.*, 81(2):739, 2009.

[62] Surjyasish Mitra and Sushanta K Mitra. Symmetric drop coalescence on an under-liquid substrate. *Phys. Rev. E*, 92(3):033013, 2015.

[63] Kaustav Chaudhury and Suman Chakraborty. Spreading of a droplet over a nonisothermal substrate: Multiple scaling regimes. *Langmuir*, 31(14):4169–4175, 2015.

[64] Frank Schellenberger, Noemí Encinas, Doris Vollmer, and Hans-Jürgen Butt. How water advances on superhydrophobic surfaces. *Phys. Rev. Lett.*, 116(9):096101, 2016.

[65] Alice C Ortmann, Jennifer Anders, Naomi Shelton, Limin Gong, Anthony G Moss, and Robert H Condon. Dispersed oil disrupts microbial pathways in pelagic food webs. *PLoS One*, 7(7):e42548, 2012.

Chapter 5

Conclusion

In this thesis, different aspects of under-liquid wetting dynamics were explored, namely coalescence of two sessile drops on an under-liquid substrate, spreading of a liquid drop on an under-liquid substrate and interaction of a liquid drop on an under-liquid micro-patterned substrate. All the studies performed here have a common underlying theme: to better understand wetting process on under-liquid surfaces with the aid of (or with appropriate modification of) existing theories on similar wetting processes in air. The goal is to create solutions to emerging problems in marine environment. As a first step, this study was aimed at better understanding of fundamentals of such wetting processes in under-liquid systems which is currently lacking in available literature. In this chapter, we briefly review our findings and propose possible directions towards future study.

On under-liquid drop coalescence

In Chapter 2, we have investigated from a theoretical perspective how two symmetric sessile drops coalesce on a substrate kept immersed in a second immiscible liquid. A modified lubrication theory has been developed to explain the coalescence dynamics. The modified theory successfully incorporated the role of both the drop liquid and surrounding liquid viscosity in dictating such a coa-

lescence process. It was shown that the early time coalescence process follows a universal dynamics in terms of growth of liquid bridge height formed upon initial contact. This was demonstrated through study of the bridge height growth for a wide range of viscosity ratio of the drop and surrounding liquid. Based on the modified lubrication theory, self similar nature of liquid bridge growth was obtained for early times of coalescence which conforms to the corresponding in air scenario. However, the self similarity observed, was for a lesser duration. The observed results indicate negligible role of the contact line during early times of coalescence.

A natural extension to the present study is the analysis of asymmetric coalescence, where the individual coalescing drops have different initial contact angles. The corresponding scenario in ambient air has been performed and well documented [1]. Further, a relevant question arising out of the present work: Is the wedge flow approximation valid for large initial contact angles? It would be interesting to investigate the dependence of initial (or equilibrium) contact angle of the merging drops on the coalescence process. Also, the lower limit of drop viscosity, which will satisfy the lubrication analysis is an interesting future work.

On experimental front, there are certain challenges which needs to be overcome to perform a detailed experimental validation of the present analysis. Most hydrophilic surfaces exhibit oleophobicity under-water [2], i.e., an oil drop on a surface immersed under-water shows an equilibrium contact angle greater than 90°. For two liquid drops with initial equilibrium contact angles greater 90°, the onset of the coalescence process is different. The logical solution would be to use hydrophobic surfaces which will show oleophilicity under-water. In the regard, most hydrophobic surfaces are made with some sort of coating (say, on glass) which makes the surface lose its transparency. Hence, the bridge dynamics from bottom view is difficult to observe for such a surface. Hence, the primary

challenge is to prepare appropriate surfaces (transparent and oleophilic) for a comprehensive experimental investigation of such coalescence process.

On under-liquid drop spreading

In Chapter 3, the spreading of oil drops on under-water glass substrates was investigated experimentally. The experimental procedure consists of imaging the fast evolution of drop contact radius over time using a high speed camera. It was demonstrated that despite the presence of a surrounding viscous medium, the initial dynamics is inherently fast due to the large Laplace pressure gradient at the moment of first contact. It was shown that for under-liquid cases, spreading always began in a viscous regime where the spreading radius grew following a scaling $r \sim t$. A switch from the initial viscous regime to a second inertial regime was observed to be dictated by the characteristic viscous length scale. Further, the corresponding spreading problem in ambient air was revisited. It was found that irrespective of the outer medium, spreading always began in a viscous regime. The role of the outer medium only showed up in the prefactor of the power law (i.e., $r \sim t$ for viscous regime and $r \sim t^{1/2}$ for the inertial one) observed and not in the exponent. It was shown that spreading always terminates in the Tanner's regime irrespective of the outer medium. Lastly, it was shown how the spreading process is truly independent of surface wettability at early times.

The early time spreading of liquid drops is inextricably linked to the coalescence analysis performed in Chapter 2 due to similarity in driving mechanism and lack of dependence on substrate wettability. The present study demonstrated the analogous nature of spreading and coalescence which can be further extended to create an unifying model to understand these two very similar aspect of surface wetting.

In the experiments performed, the initial impact speed of the drop touching the surface was kept as low as possible to avoid any unwarranted drop defor-

mation. It would be interesting to vary the initial impact speed, hence impact Weber No. and study its effect on the wetting dynamics. Further, a detailed theoretical investigation of the exact mechanism of liquid-liquid displacement for early times of under-liquid spreading makes an interesting future scope.

On wetting of under-liquid micro-patterned substrates

In Chapter 4, the wetting behavior of oil drops on micro-patterned substrates placed under-water was studied experimentally. It was demonstrated that conventional theories of Wenzel and Cassie-Baxter fails to accurately capture the wetting behavior. This was concluded due to discrepancies in the observed contact angle values (static, advancing and receding) with those predicted by the theories. It should be noted here that we do not propose to completely disregard those theories. We only point to the fact that these wetting theories do not take into account various aspects like wetting transition, dynamics of liquid-liquid displacement, etc which are major considerations in studying such under-liquid systems.

The natural future extension to this study is to perform a theoretical analysis to quantify the wetting behavior on under-water textured surfaces. This would warrant the need of rigorous computation to understand the exact mechanism of wetting transition. Recently, using atomistic simulations, some light has been thrown on this complex issue of wetting transition on textured surfaces kept in air[3]. On similar lines, computational analysis can be performed to better understand this issue on under-liquid systems.

Bibliography

[1] JF Hernández-Sánchez, LA Lubbers, Antonin Eddi, and JH Snoeijer. Symmetric and asymmetric coalescence of drops on a substrate. *Phys. Rev. Lett.*, 109(18):184502, 2012.

[2] Yong Chae Jung and Bharat Bhushan. Wetting behavior of water and oil droplets in three-phase interfaces for hydrophobicity/philicity and oleophobicity/philicity. *Langmuir*, 25(24):14165–14173, 2009.

[3] Alberto Giacomello, Mauro Chinappi, Simone Meloni, and Carlo Massimo Casciola. Metastable wetting on superhydrophobic surfaces: continuum and atomistic views of the cassie-baxter–wenzel transition. *Phys. Rev. Lett.*, 109(22):226102, 2012.

List of Publications

Journal Papers Published

1. **S. Mitra** and S. K. Mitra, Symmetric drop coalescence on an under-liquid substrate, *Physical Review E*, 92(3) , 033013, 2015.

2. P. R. Waghmare, **S. Mitra**, N. S. K. Gunda and S. K. Mitra, Needle-free drop deposition: the role of elastic membranes, *RSC Advances*, 5(100), 82374-82380, 2015.

3. **S. Mitra** and S. K. Mitra, Understanding the early regime of drop spreading, *Langmuir*, DOI: 10.1021/acs.langmuir.6b02189, 2016. .

Manuscript Under Preparation

1. **S. Mitra**, N. S. K. Gunda and S. K. Mitra,, Wetting characteristic of under-liquid micro-patterned substrates: Is Wenzel and Cassie-Baxter still valid?.

Conference Proceedings

(a) **S. Mitra**, N. S. K. Gunda and S. K. Mitra, Under-water wetting behavior on micro-patterned substrates, Paper # ICNMM2016-7941, Proceedings of ASME 2016 14th International Conference on Nanochannels, Microchannels and Minichannels, ICNMM 2016, Washington DC, USA, July 10-14, 2016.

Oral Presentations

(a) **S. Mitra** and S. K. Mitra, Dynamics of drop coalescence on under liquid substrates, Paper # L35.005, APS 68th Annual DFD Meeting,

Boston, USA, November 22-24, 2015.

(b) N. S. K. Gunda, **S. Mitra** and S. K. Mitra, Drop spreading on under-liquid substrates: Inertial to Viscous Regimes, Paper # R33.006, APS 68th Annual DFD Meeting, Boston, USA, November 22-24, 2015.

Poster Presentations

i. **S. Mitra** and S. K. Mitra, Symmetric drop coalescence on under liquid substrates, 5th International Colloids Conference, Amsterdam, Netherlands, June 21-24, 2015.

ii. **S. Mitra** and S. K. Mitra, Wetting Dynamics on under-liquid substrates. XXIV International Conference on Theoretical & Applied Mechanics, ICTAM, Montreal, Canada, . August 21-26, 2016. To be presented.

Appendix A

Detailed expressions

Detailed expressions for $f_1(\theta)$ and $f_2(\theta)$

$$f_1(\theta) = \frac{1}{(\beta^2 - cos^2\theta)(cos^3\theta + \beta sin\theta cos^2\theta)} \left[sin^2\theta cos^3\theta \right.$$
$$\left. -\beta cos^2\theta \left\{ (1+sin\theta)^2 + cos\theta \right\} + \beta^2 (2sin\theta cos\theta + sin^2\theta) \right] \tag{A.1}$$

$$f_2(\theta) = \frac{1}{(\beta^2 - cos^2\theta)(cos^3\theta + \beta sin\theta cos^2\theta)} \left[\beta^3 sin^2\theta cos^3\theta \right.$$
$$+\beta^2 \left(2sin^3\theta - sin^2\theta cos\theta\right) + \beta sin\theta \left(sin^3\theta + 2cos^3\theta\right)$$
$$\left. +2sin^2\theta cos^3\theta - sin^2\theta - cos^4\theta \right] \tag{A.2}$$

where $\theta(t)$ is the gradually diminishing wedge angle and $\beta(t) = \pi/2 - \theta(t)$.

Appendix B

Derivation of lubrication equation in air

The governing equation describing the coalescence behavior of two liquid drops on a substrate can be derived from the creeping flow assumption of the Navier Stokes' equation. The liquids are Newtonian with a density ρ_D and viscosity μ_D. The velocity and pressure fields are denoted by u_D and p_D, respectively. The continuity and momentum equations can be written as,

$$\nabla u_D = 0 \tag{B.1}$$

$$\nabla^2 u_D = \nabla p_D \tag{B.2}$$

subjected to boundary conditions: no-slip at the substrate,

$$u_D = 0 : z = 0 \tag{B.3}$$

and

$$\frac{\partial u}{\partial z} = 0 : z = h(x,t) \tag{B.4}$$

On applying the boundary conditions, we get

$$u(x,z,t) = -\frac{1}{2\mu} z(2h(x,t) - z)\gamma \frac{\partial p}{\partial x} \tag{B.5}$$

The volumetric flow rate (per unit width) can be written as,

$$Q = \int_0^h u(x,z,t)dz = -\frac{1}{3\mu} h^3 \frac{\partial p}{\partial x} \tag{B.6}$$

The pressure field can be derived from the Laplace equation as,

$$p(x,z,t) = \gamma \frac{\partial^2 h}{\partial^2 x} \tag{B.7}$$

Now applying mass conservation,

$$\frac{\partial h}{\partial t} + \frac{\partial Q}{\partial x} = 0 \tag{B.8}$$

we get the lubrication equation for describing the coalescence of sessile drops,

$$\frac{\partial h}{\partial t} + \frac{\gamma}{3\mu_D} \frac{\partial}{\partial x} \left(h^3 \frac{\partial^3 h}{\partial x^3} \right) = 0 \tag{B.9}$$

Appendix C

Derivation of capillary length for under-liquid systems

Consider an interface separating a liquid drop of uniform density ρ_D in another liquid medium with uniform density ρ_L. Considering the system to be at rest, the pressure in the liquid drop varies as $p_D = p_L - \rho_L g z$ where, g is the acceleration due to gravity and z measures vertical height (relative to the equilibrium height of the interface in the absence of surface tension). Hence, the Young-Laplace equation yields,

$$(\rho_D - \rho_L) g z = -\gamma \nabla . \mathbf{n} \tag{C.1}$$

where $\mathbf{n}$ is the normal to the interface directed from liquid to air. If R is the typical radius of curvature of the interface then the left-hand side of the above equation dominates the right-hand side whenever $R \gg l$, and vice versa. Here, l is the capillary length scale given as,

$$l = (\frac{\gamma}{(\rho_D - \rho_L) g})^{1/2} \tag{C.2}$$

C.1 Drop sizes used in the present study

For the liquids used in the present work i.e., laser oil and DBP, the capillary length scales under-water are 7mm and 7.05mm, respectively. Hence, the consideration of 0.7 mm radius drops for the experiments to neglect gravity effects is valid.